

Introduction to Himawari-8 RGB composite imagery

SHIMIZU Akihiro*

Abstract

Imagery produced by the multi-spectral visible and infrared Advanced Himawari Imager (AHI) on board JMA's Himawari-8 satellite provides much more physical information than the heritage imagers on board the previous GMS and MTSAT series of satellites due to its increased observation bands. In this context, the red-green-blue (RGB) composite technique is applied for appropriate utilization of data provided from multiple spectral bands. RGB composite imagery, produced with focus on the global standards recommended by the World Meteorological Organization (WMO), is widely used by forecasters and researchers worldwide. This report outlines the RGB composite technique and its application to Himawari-8 imagery, with coverage of widely used RGB data and new RGB composite imagery developed by the Japan Meteorological Agency (JMA).

1. Introduction

The current Himawari-8/9 geostationary satellites each carry a multi-spectral Advanced Himawari Imager (AHI), which has 15 observation bands as compared to the 5 bands (channels) of the previous-generation MTSAT-1R/2 (Multi-functional Transport Satellite) units (Table 1). This enhancement provides large amounts of information from individual characteristic bands (e.g., Band 4 for vegetation and Band 12 for ozone absorption; Clerbaux, 2011). Principally, previous usage involved limited numbers of single grayscale and color-enhanced images (Shimizu et al, 2017), but such usage is now considered sub-optimal for implementation with tight deadlines (e.g., in the provision of urgent weather warnings).

The RGB composite technique involves the utilization of multiple spectral images based on the assignment of red, green and blue (the three primary colors of light) to satellite images and application of color representation based on an additive mixture of colors. With suitable color schemes (i.e., combinations of imagery for assignment of the three primary colors) and

thresholds, RGB composite imagery can be used to display surface and atmospheric conditions/phenomena as described below.

Table 1: Observation bands of Himawari-8 and -9, MTSAT-1R and -2 and MSG, and related physical properties for imagery

Band	Himawari-8/-9	MTSAT-1R/-2	MSG	Physical Properties for Imagery	
1	0.47 μm			Aerosol B	Visible
2	0.51 μm			Aerosol G	
3	0.64 μm	0.68 μm	0.635 μm	Low cloud, fog R	
4	0.86 μm		0.81 μm	Vegetation, aerosol	Near Infrared
5	1.6 μm		1.64 μm	Cloud phase	
6	2.3 μm			Particle size	
7	3.9 μm	3.7 μm	3.9 μm	Low cloud, fog, forest fire	Infrared
8	6.2 μm	6.8 μm	6.2 μm	Upper level moisture	
9	6.9 μm			Mid- upper level moisture	
10	7.3 μm		7.3 μm	Mid-level moisture	
11	8.6 μm		8.7 μm	Cloud phase, SO ₂	
12	9.6 μm		9.7 μm	Ozone content	
13	10.4 μm	10.8 μm	10.8 μm	Cloud imagery, information of cloud top	
14	11.2 μm			Cloud imagery, sea surface temperature	
15	12.4 μm	12.0 μm	12.0 μm	Cloud imagery, sea surface temperature	
16	13.3 μm		13.4 μm	Cloud top height	

*Satellite Application and Analysis Division, Data Processing Department, Meteorological Satellite Center

(Received 11 November 2018, accepted 30 October 2020)

In this way, users can obtain various types of information simultaneously via RGB composite imagery, which also supports expert users in the analysis of grayscale satellite imagery with extra information on variables such as cloud shape and texture. The RGB composite method additionally plays a part in quantitative assessment of geophysical products output by researchers and developers and in routine forecasting work (WMO, 2012).

The multi-spectral Spinning Enhanced Visible and Infrared Imager (SEVIRI) on board the European Meteosat Second-Generation (MSG) geostationary satellite has been operated since 2004 by EUMETSAT, and features more bands (with 12 channels including broadband (approx. 0.4 – 1.1 μm) visible) than other imagers on board former geostationary earth orbit (GEO) meteorological satellites. MSG users are already familiar with the RGB composite technique from the application of MSG imagery, and many of the practical MSG RGB recipes (Kerkmann 2005, Lensky and Rosenfeld 2008, EUMeTrain 2017 – 2018) provided by EUMETSAT are used as WMO standard schemes (WMO 2007, 2012). Since AH1 observation bands are configured in the same (or similar) ways as SEVIRI channels, MSG RGB recipes are applicable for appropriate combinations of Himawari imagery. Against this background, JMA introduced EUMETSAT RGB schemes into RGB compositing using Himawari-8 imagery, thereby allowing Himawari users to apply the same color interpretation guide as MSG users. The Agency also adopted LEO (low-earth-orbit) meteorological satellite RGB schemes as well as developing its own such schemes.

2. Basics of the RGB composite technique

As described above, RGB composite imagery is composed of multiple images assigned to the three primary colors of red, green and blue. In

the RGB model, representation is based on contributions from each color. To reproduce various hues, a 24-bit (three 8-bit values as integer numbers in the range from 0 to 255) computer color model is applied to the RGB composite technique for satellite imagery. As red-green-blue images each have values of 256 ($= 2^8$) (8-bit) shades, 256^3 ($= 2^{8*3} = 16,777,216$) (24-bit) colors can be displayed in RGB composite imagery (Fig. 1).

Depending on the purpose of use, it is necessary to select single or channel difference images for RGB assignment to adjust the relevant thresholds (e.g., brightness temperature (TBB)/reflectivity and gamma values) for RGB imagery compositing.

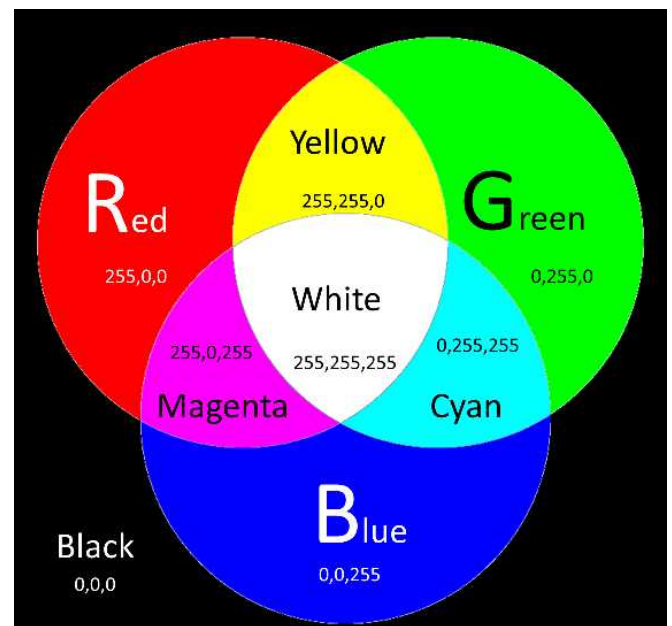


Fig. 1: RGB color model based on additive color mixing. Numbers indicate related RGB 8-bit values.

2.1. Selection of images for RGB assignment

Images with three-color components are determined for focus on cloud conditions (e.g., lower or upper, cloud particle size, phase) and other phenomena (e.g., dust, volcanic ash, gas)

within single or different images. For example, if RGB composite imagery with higher brightness temperatures (TBBs) in a bluish shade is required, Band 13 (10.4 μm) imagery is appropriate for the blue component. In this case, the inverse image of the usual gray-scale Band 13 imagery is applied, meaning that pixels with higher TBBs will be displayed more brightly.

RGB scheme allocation is also important for highlighting clouds and phenomena. If three images are applied in RGB composition, there are six combinations for red, green and blue beams. To support visual perception, warning colors such as red/yellow and natural colors such as green for vegetation are considered according to purpose (Fig. 2).

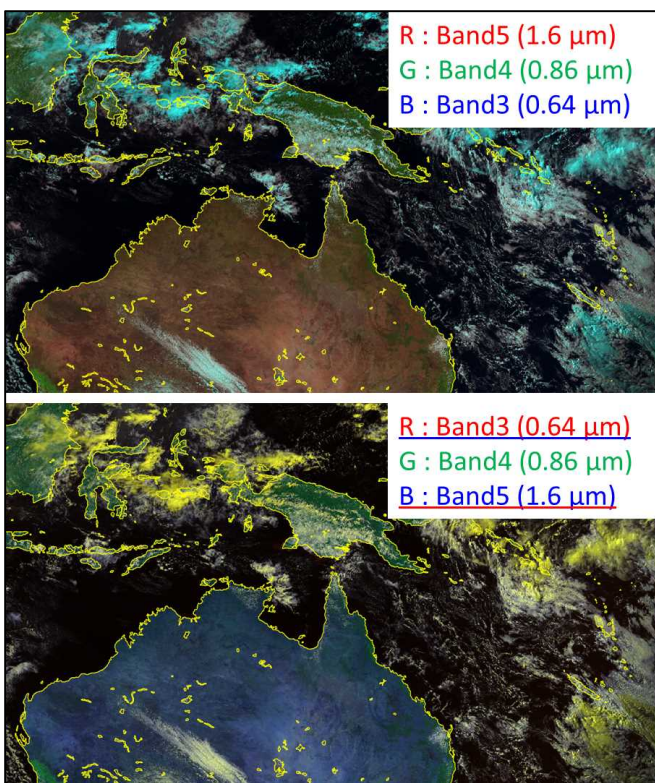


Fig. 2: Comparison of differences of bands assigned to RGB colors. This genuine Natural Color RGB scheme imagery supports visualization of surface conditions.

Against this background, a basic grounding in imagery characteristics is necessary to improve

existing RGB composites and design new composites. Accordingly, it is important to effectively use WMO standard schemes or EUMETSAT RGB composites as detailed below.

2.2. Threshold adjustment

Individual images used in RGB composites display clouds and phenomena based on the relevant characteristics. Satellite image users often adjust image color contrast and brightness to highlight specific clouds or phenomena, and such manipulation plays a key role in ensuring the desired RGB display characteristics. For satellite imagery, the thresholds for the ranges of TBB /reflectivity and gamma value correction are required.

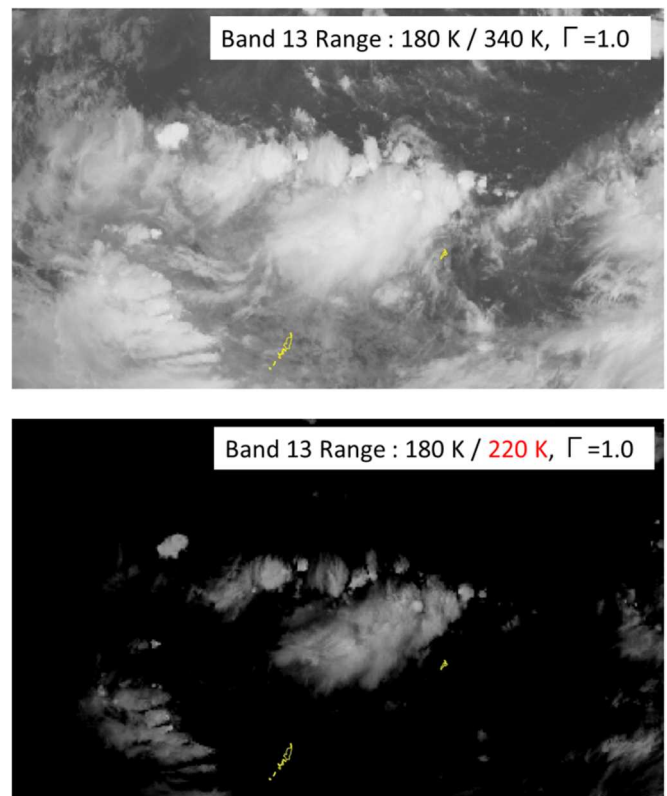


Fig. 3: Example of brightness temperature adjustment in Band 13 infrared imagery

Figure 3 shows an example involving brightness temperature adjustment. The upper image (Band 13; 10.4 μm ; TBB range: 180 – 340 K) shows

developing Cb (cumulonimbus) clouds together with various types of high-level cirrus cloud and mid/low-level cloud. To highlight Cb cloud, the TBB range needs to be adjusted because the cloud top is very cold. Narrowing this range to a lower threshold emphasizes Cb in the bottom image (10.4 μm; TBB range: 180 K – 220 K).

Gamma value correction is also effective in highlighting specific clouds and phenomena via enhancement of high/low brightness intensity (0 – 255) pixel values (BYTE). The formula for such correction is

$$BYTE = 255 * \left[\frac{(TBB,REF) - MIN}{MAX - MIN} \right]^{\frac{1}{\Gamma}} \quad (1)$$

where TBB is brightness temperature (for infrared imagery), REF is reflectivity (for visible and near-infrared imagery), MIN and MAX represent the ranges of brightness temperature/reflectivity, and Γ is the gamma value.

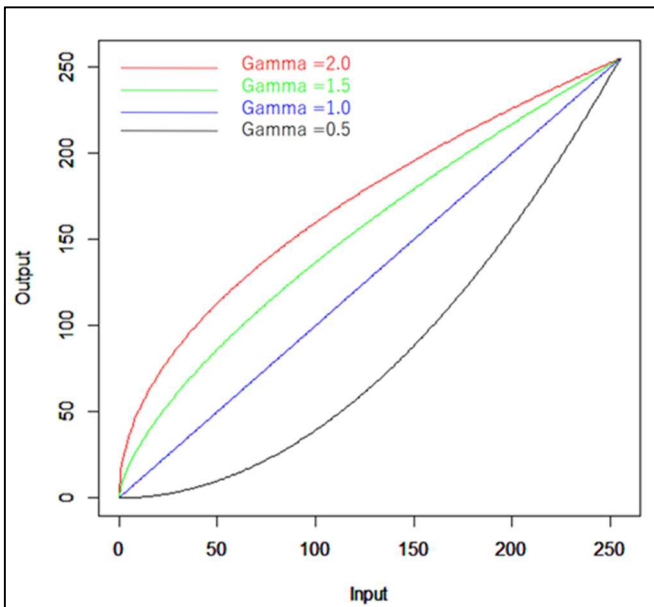


Fig. 4: Plotted correction functions for different gamma values

Figure 4 shows the input-output relationship for different gamma values. Gamma correction

gives image pixel values a non-linear spread. This results in darkening for gamma values of < 1.0, which particularly affects already-dark (low-input) pixels, and the contrast of the part of higher/lower pixels are enhanced by the correction of >1.0. Figure 5 shows an example involving gamma value adjustment.

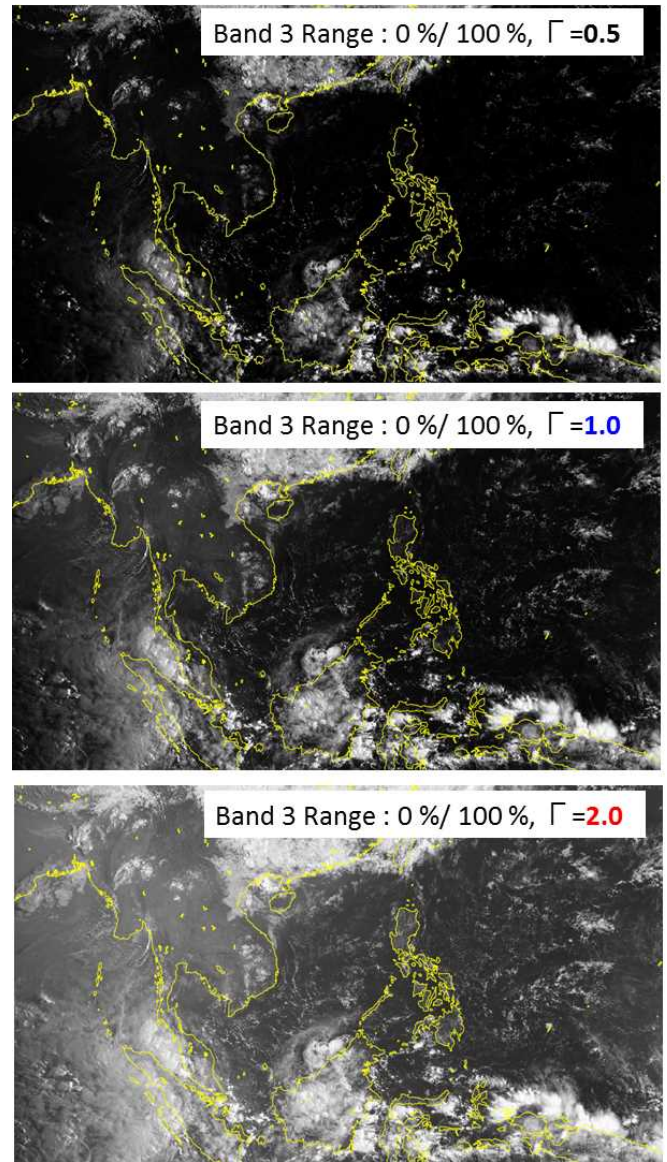


Fig. 5: Example of gamma value adjustment in Band 3 visible imagery. Thick clouds are highlighted at $\Gamma = 0.5$, while thin high clouds and land surfaces are emphasized at $\Gamma = 2.0$.

3. Main objectives of RGB composites and widely used RGB composite schemes

As described above, EUMETSAT RGB composites are well known and widely used with schemes providing multi-spectral imager support for the derivation of qualitative information on:

- Radiating surface temperature (ground or cloud top)
- Cloud particle phase (ice or water)
- Cloud particle relative size
- Cloud optical depth
- Cloud height
- Aerosols (e.g., smoke, dust, volcanic ash)
- Air mass type in the middle/upper troposphere with stratospheric ozone content
- Vertical moisture distribution
- Surface type (e.g., snow cover, vegetation)
- Surface hot spots (e.g., wildfires)

Table 2 lists widely used RGB composites and recommended thresholds for Himawari-8. As MSG imagery thresholds sometimes do not work well with Himawari-8 imagery due to subtle spectral band differences between SEVIRI and AHI observation data, threshold values are adjusted (Fig. 6). For information on the original MSG RGB thresholds, see Appendix 1. The adjusted values are derived from comparison of simulation data between SEVIRI and AHI (Murata and Shimizu, 2017).

It is also necessary to adjust the reflectivity of the visible and near-infrared bands by the cosine of the solar zenith angle to enhance dawn/dusk and high-latitude region imagery.

Based on such correction, Himawari RGB users can apply the same color interpretation guide as MSG users. However, colors do not always match exactly because those based on signals from individual components may vary diurnally, seasonally and latitudinally in

addition to differences among imagers.

Table 2: Widely used RGB composites and recommended thresholds for Himawari-8

	H8 Bands	Central wave length [μm]	Min [K/%]	Max [K/%]	Gamma
Natural color RGB					
R	B05	1.6	0%	99%	1.0
G	B04	0.86	0%	102%	0.95
B	B03	0.64	0%	100%	1.0
True color RGB					
R	B03	0.64	0%	100%	1.0
G	B02	0.51	0%	100%	1.0
B	B01	0.47	0%	100%	1.0
Day Snow-Fog RGB					
R	B04	0.86	0%	102%	1.6
G	B05	1.6	0%	68%	1.7
B	B07refl	3.9	2%	45%	1.95
Day microphysics RGB (Summer/Winter)					
R	B04	0.86	0%	102%	0.95
G	B07refl	3.9(summer) /3.9(winter)	2% /2%	82% /38%	2.6 /1.8
B	B13 (inverse)	10.4	203.5K	303.2K	1.0
Day convective storms RGB					
R	B10-B08	7.3-6.2	-5.0K	36.0K	1.0
G	B13-B07	10.4-3.9	-1.0K	61.0K	0.5
B	B03-B05	0.64-1.6	-80%	26%	0.95
Night microphysics RGB					
R	B13-B15	10.4-12.4	-3.0K	7.5K	1.0
G	B07-B13	3.9-10.4	-7.0K	2.9K	1.0
B	B13 (inverse)	10.4	243.7K	293.2K	1.0
24-hour microphysics RGB					
R	B13-B15	10.4-12.4	-3.0K	7.5K	1.0
G	B11-B13 /B11-B14	8.6-10.4 /8.6-11.2	0.8K -0.4K	5.8K 6.1K	1.3 1.1
B	B13 (inverse)	10.4	248.6K	303.2K	1.0
Dust RGB					
R	B13-B15	10.4-12.4	-3.0K	7.5K	1.0
G	B11-B13 /B11-B14	8.6-10.4 /8.6-11.2	0.9K -0.5K	12.5K 15.0K	2.5 2.2
B	B13 (inverse)	10.4	261.5K	289.2K	1.0
Ash RGB					
R	B13-B15	10.4-12.4	-3.0K	7.5K	1.0
G	B11-B13 /B11-B14	8.6-10.4 /8.6-11.2	-1.6K -5.9K	4.9K 5.1K	1.2 0.85
B	B13 (inverse)	10.4	243.6K	303.2K	1.0
Airmass RGB					
R	B10-B08	7.3-6.2	0.0K	25.8K	1.0
G	B13-B12	10.4-9.6	-4.3K	41.5K	1.0
B	B08	6.2	208.0K	242.6K	1.0

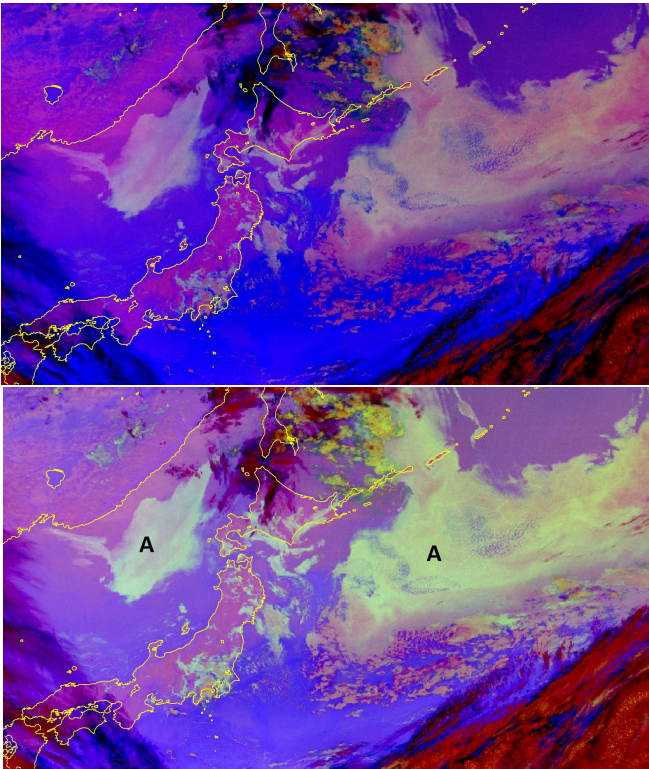


Fig. 6: Example of comparison between Night Microphysics RGB with MSG thresholds (no adjustment; top) and adjusted thresholds for AHI/Himawari-8 (bottom). Color tones of bright greenish clouds (marked “A”) corresponding to low-level clouds show particular improvement in RGB imagery.

3.1. Natural Color (Day Natural Color) RGB

Natural Color RGB is useful for determining

surface characteristics (snow, vegetation, bare soil) and cloud particle phases (ice cloud, water cloud). In such application, red, green and blue are assigned to imagery from Band 5 (1.6 μm), Band 4 (0.86 μm) and Band 3 (0.64 μm). Bands 5 and 4 have near-infrared observation specifications, and Band 3 is a visible channel. All three have characteristic and useful reflection properties allowing the distinction of ice/water clouds and determination of ground surface conditions such as coverage with snow/ice and vegetation (Table 3).

Typical color interpretation and RGB values (three 8-bit colors and HTML color codes) inherited from EUMETSAT are shown in Table 4. The greater reflectance for vegetation in Band 4 for green components produces a greenish hue in imagery. Dense clouds containing water droplets exhibit high reflectance in all three components, resulting in a whitish or bright-greyish manifestation. Ice clouds have lower reflectance in Band 5 for the red component, meaning that the green and blue components produce a cyan effect. This also applies to the color of snow- or ice-covered surfaces. Bare soil surfaces such as desert terrain reflect incident light comparatively well in Band 5, and hence the brown/reddish color corresponds to such surfaces.

The top image in Fig. 7 shows a situation with low-level clouds including fog (in bright-greyish, marked “C”) drifting toward southeastern

Table 3: Band components and related specifications for Natural Color RGB

Color	AHI Bands	Central wave length [μm]	Physically relates to	Smaller contribution to the signal of	Larger contribution to the signal of
Red	B05	1.6	Cloud phase Snow and ice	Ice clouds Snow covered land/sea ice	Water clouds
Green	B04	0.86	Cloud optical thickness Green vegetation	Thin clouds	Thick clouds Snow covered land Vegetation
Blue	B03	0.64	Cloud optical thickness	Thin clouds	Thick clouds Snow covered land Sea ice

Table 4: Color interpretation and RGB values for Natural Color RGB

Color	Interpretation	RGB Value	HTML
	High-level ice clouds	77,205,205	#4DCDCD
	Low-level water clouds	220,200,200	#DCC8C8
	Ocean	8,9,15	#08090F
	Vegetation	66,133,46	#42852E
	Desert	173,126,103	#AD7E67
	Snow/Ice	21,233,221	#15E9DD

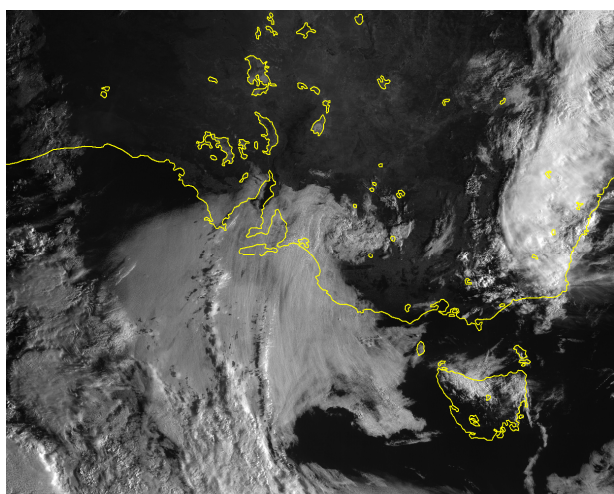
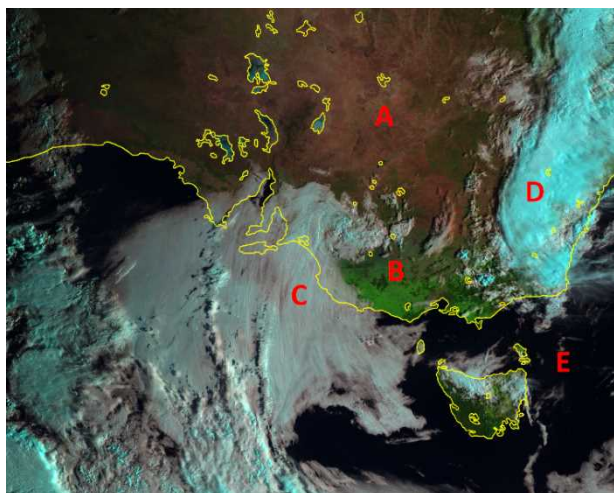


Fig. 7: Low-level clouds including fog drifting toward southeastern Australia (2100 UTC, 17 November 2017). Top: Natural Color RGB imagery; bottom: visible (Band 3) imagery.

A: bare ground or desert; B: vegetation; C: thick low-level cloud; D: thick high-level cloud; E: ocean

Australia. Due to Band 5's lesser contribution to pixels for ice cloud particles, the high-level ice cloud (marked "D") appears in cyan as a result of contributions from green and blue.

In this way, Natural Color RGB facilitates distinction between ice cloud and water cloud, and between areas of snow cover and vegetation. Such imagery is available only from daytime observation due to dependence on solar (visible and near-infrared) band imagery.

3.2. True Color RGB

True Color RGB involves the use of the visible-light Bands 1 (0.47 μm), 2 (0.51 μm) and 3 (0.64 μm) in the order of red, green and blue (Table 5), allowing the display of colors visible to the naked eye. However, a value of 0.555 μm (in contrast to the native 0.51 μm) is optimal for the green component. By way of example, the much lower reflectance for vegetation at 0.51 μm is particularly distinctive. Accordingly, true color RGB based on these native color bands looks somewhat unnatural, but allows intuitive understanding of surface and atmospheric conditions.

All cloud types in imagery (Fig. 8) appear in simple whitish tones with three visible bands, and areas of coverage with snow/ice and clouds both appear in bright white. This RGB scheme is consequently not suitable for detailed cloud and surface analysis, but provides favorable sensitivity for aerosols such as smoke, dust and volcanic ash (Figs. 8 and 9).

Table 5: Band components and related specifications for True Color RGB

Color	AHI Bands	Central wave length [μm]	Physically relates to	Smaller contribution to the signal of	Larger contribution to the signal of
Red	B03	0.64	Cloud optical thickness Snow and ice	Thin clouds	Thick clouds Snow covered land Sea ice
Green	B02	0.51	Cloud optical thickness Snow and ice	Thin clouds	Thick clouds Snow covered land Sea ice
Blue	B01	0.46	Cloud optical thickness Snow and ice	Thin clouds	Thick clouds Snow covered land Sea ice

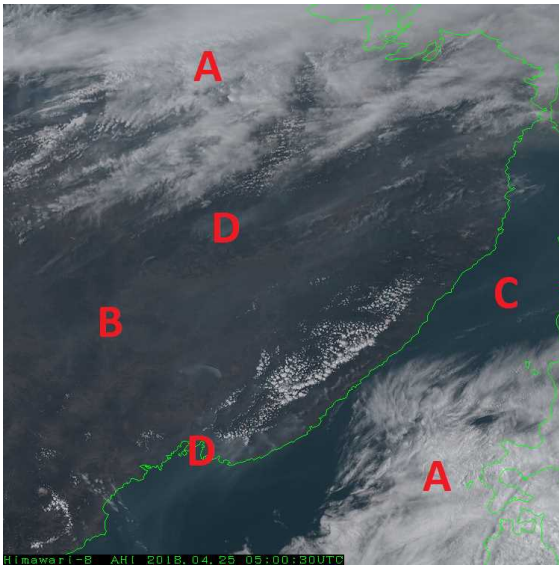


Fig. 8: Forest-fire smoke around Siberia (0500 UTC, 25 April 2018)

A: cloud; B: land surface; C: sea surface; D: smoke

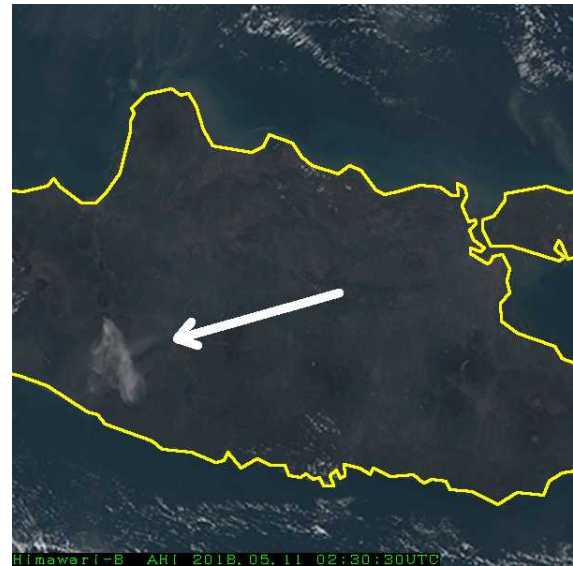


Fig. 9: Eruption of Mt. Merapi, Indonesia (0230 UTC, 11 May 2018)

The white arrow indicates a volcanic ash plume.

3.3. Day Snow-fog RGB

Day Snow-fog RGB is a useful composite scheme for distinguishing daytime coverage with snow/ice and fog/low cloud. This RGB scheme is composed of Bands 4 (0.86 μm), 5 (1.6 μm) and the solar component of Band 7 (3.9 μm) in the red, green and blue beams, respectively. Band 7 observation involves both emitted thermal radiation and reflected solar radiation for the daytime. Due to these respective contributions, Band 7 imagery is complex in relation to daytime usage, but reflected solar radiation (i.e., the solar component) is characterized by remarkable

Table 6: Band components and related specifications for Day Snow-fog RGB

Color	AHI Bands	Central wave length [μm]	Physically relates to	Smaller contribution to the signal of	Larger contribution to the signal of
Red	B04	0.86	Cloud optical thickness Snow and ice	Thin clouds	Water clouds Snow covered land/sea ice
Green	B05	1.6	Cloud phase (and size) Snow and ice	Ice clouds with large ice crystals Snow covered land/sea ice	Thick water clouds with small droplets
Blue	B07refl	3.9	Cloud phase and size Snow and ice	Ice clouds with large ice crystals Snow covered land/sea ice	Thick water clouds with small droplets

Table 7: Color interpretation and RGB values for Day Snow-fog RGB

Color	Interpretation	RGB Value	HTML
	Deep precipitating cloud (precip. not necessarily reaching the ground) - bright, thick, large ice particles	200,140,50	#C88C32
	Deep precipitating cloud (or thick, high-level lee cloudiness with small ice particles) - bright, thick, small ice particles	220,200,120	#DCC878
	Thick water cloud with large droplets	220,210,190	#DCD2BE
	Thick water cloud with small droplets	250,250,250	#FAFAFA
	Ocean	25,18,51	#191233
	Vegetation	120,150,100	#789664
	Desert	140,220,240	#8CDCF0
	Snow/Ice	240,90,25	#F05A19

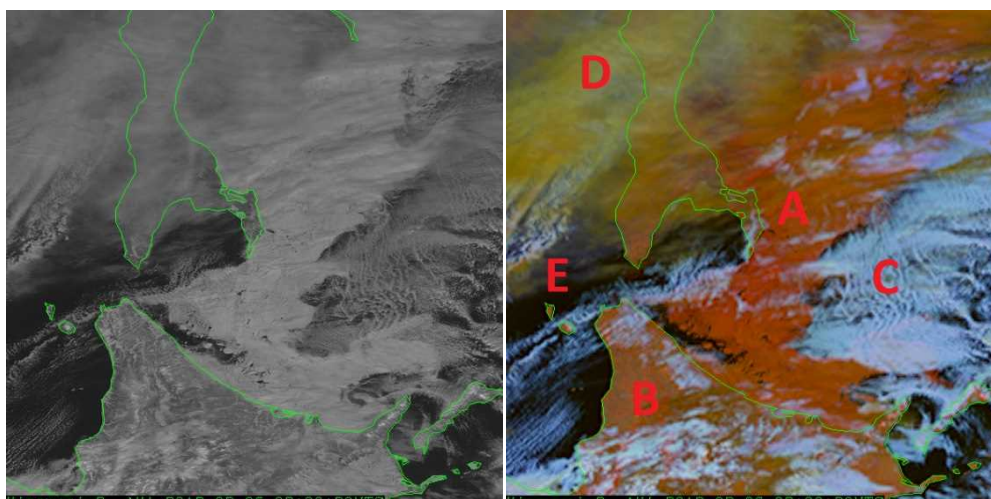


Fig. 10: Sea ice around the Sea of Okhotsk, northern Japan and Russia (0300 UTC, 6 February 2018). Left: Day Snow-fog RGB imagery; right: visible (Band 3) imagery
A: sea ice; B: snow-covered land; C: low-level water cloud; D: high-level cloud with small ice particles; E: sea surface

reflective properties for cloud particle size and phase. Small water droplets exhibit high

reflectance, while large ice crystals show low reflectance in the solar component of Band 7

(Table 6).

To emphasize these characteristics, imagery based on the Band 7 solar component can be derived via approximate calculation with other band data (see Appendix 2).

Color interpretation for Day Snow-fog RGB is shown in Table 7. The green beam of Band 5 and the blue beam of Band 7 (the solar component) have low reflectivity for coverage with snow and ice, respectively, producing a reddish hue in the coverage area. Meanwhile, optically thick water clouds (including fog) show high reflectance in all three components, causing water clouds to appear whitish. Distinction between low cloud/fog and snow-covered land/sea ice is thus easier than with single visible band imagery (A and C in Fig. 10), for instance. Reflective properties based on information from Band 7 (solar component) and Band 5 provide useful information on cloud top particle states with phenomena such as small ice crystals. High-level clouds appear in ocher (D in Fig. 10). Clouds around these areas appear translucent, suggesting thin high-level manifestation with small ice particles.

3.4. Day Microphysics RGB

Day Microphysics RGB allows detailed cloud analysis for daytime conditions. In this scheme, the Band 7 solar component is incorporated as green-beam content. Band 4 (0.86 μm) and Band 13 (10.4 μm) are assigned as the red- and blue-beam content for the scheme, respectively (Table 8).

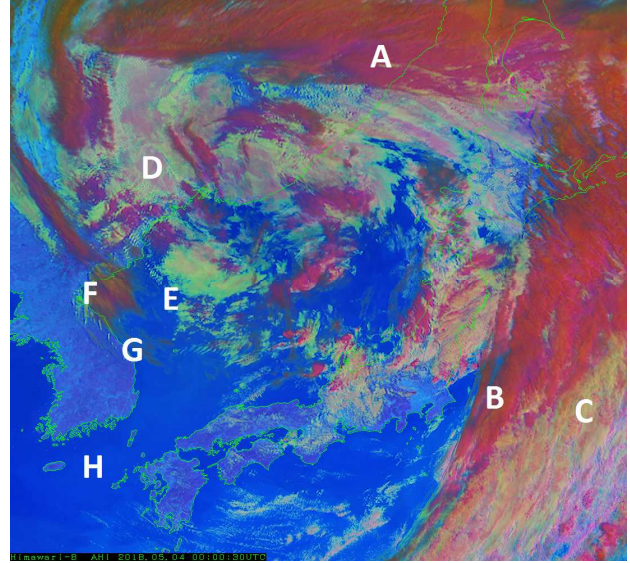


Fig. 11: Cloud areas with a polar low-pressure system around the Sea of Japan (0000 UTC, 4 May 2018)

A: thick cloud with large ice particles; B: thick cloud with small ice particles (including Cb cloud with strong updrafts); C: thick water cloud with super-cooled small droplets; D: thick water cloud with large droplets; E: thin water cloud with super-cooled small droplets; F: high-level lee cloudiness with small ice particles; G: thin cirrus cloud; H: sea surface

The red beam of Band 4 contributes cloud optical thickness, and the green beam of Band 7 (solar component) depends on the particle size and phase of the cloud top as described above. The blue beam of Band 13 shows information on surface and cloud top temperatures. In contrast to the situation with typical (single gray-scale)

Table 8: Band components and related specifications for Day Microphysics RGB

Color	AHI Bands	Central wave length [μm]	Physically relates to	Smaller contribution to the signal of	Larger contribution to the signal of
Red	B04	0.86	Cloud optical thickness	Thin clouds	Thick clouds
Green	B07refl	3.9	Cloud phase and size Snow and ice	Ice clouds with large ice crystals	Water clouds with small droplets
Blue	B13 (inverse)	10.4	Temperature	Cold thick clouds	Warm clouds Warm surface

Table 9: Color interpretation and RGB values for Day Microphysics RGB

Color	Interpretation	RGB Value	HTML
	Deep precipitating cloud (precip. not necessarily reaching the ground) - bright, thick, large ice particles, cold cloud	230,20,0	#E61400
	Deep precipitating cloud (Cb cloud with strong updrafts and severe weather)* - bright, thick, small ice particles, cold cloud *or thick, high-level lee cloudiness with small ice particles	205,150,35	#CD9623
	Thin Cirrus cloud (large ice particles)	80,20,40	#501428
	Thin Cirrus cloud (small ice particles)	80,150,40	#42852E
	Supercooled, thick water cloud - bright, thick, small droplets	230,250,100	#E6FA64
	Supercooled, thick water cloud - bright, thick, large droplets	230,150,100	#E69664
	Supercooled thin water cloud with large droplets	80,150,120	#509678
	Supercooled, thin water cloud with small droplets	80,250,120	#50FA78
	Thick water cloud (warm rain cloud) - bright, thick, large droplets	180,100,180	#B464B4
	Thick water cloud (no precipitation) - bright, thick, small droplets	220,250,180	#D2EFAC
	Thin water cloud with large droplets	120,100,180	#7864B4
	Thin water cloud with small droplets	120,150,180	#7896B4
	Ocean	0,0,200	#0000C8
	Vegetation	50,50,250	#3232FA
	Desert/Fire (Hot Spot)	50,255,255	#32FFFF
	Snow/Ice	250,0,127	#FA007F

infrared imagery, higher temperatures (e.g., those of ocean areas) manifest as brighter blue pixels, and lower temperatures (e.g., Cb (cumulonimbus top) manifest as darker pixels in RGB (i.e., inverted IR imagery). The various combinations of these contributions produce varied color indications and related interpretations.

Color interpretation for Day Microphysics RGB is shown in Table 9. Thick ice clouds with large particles appear reddish due to high contribution from the red beam of Band 4 and low contributions from the green beam of Band 7 (solar component) and the blue beam of Band 13. Thick ice clouds with small particles appear orange or bright brown due to high contribution from Band 4, medium contribution from Band 7 and low contribution from Band 13. High-level lee cloudiness caused by topographical ascent appears in similar hues due to its content of small

ice particles (“F” in Fig. 11).

Water clouds with very cold droplets (known as super-cooled water clouds) also influence color interpretation. Thick super-cooled clouds with small droplets appear yellowish due to high contributions from Bands 4 and 7 and low contribution from Band 13. Thin super-cooled clouds with large droplets are dark green due to medium contribution from Band 7 and low contributions from Bands 4 and 13.

Certain colors for warm water clouds apply in interpretation. Thick warm water clouds with large droplets appear purplish due to high contributions from Bands 4 and 13 and low contribution from Band 7. Thin water clouds with small droplets appear greyish-blue due to medium-to-high contributions from Bands 7 and 13 and low contribution from Band 4.

In the area of surface conditions, snow/ice coverage appears pinkish due to high

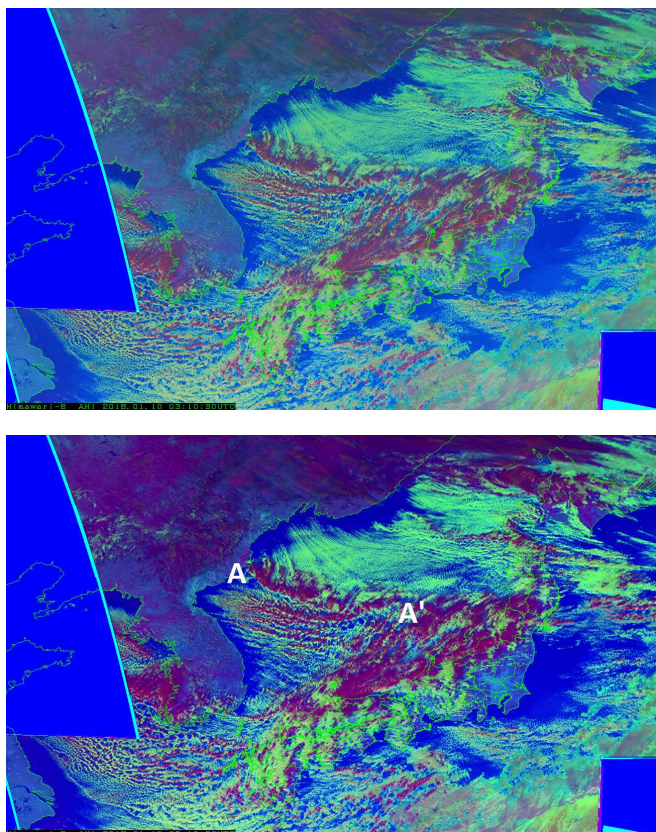


Fig. 12: Characteristic winter cloud pattern around the Sea of Japan (0310 UTC, 10 January 2018)

Top: normal (or summer) Day Microphysics RGB; bottom: Day Microphysics RGB with thresholds for winter in mid-high latitudes. The reddish cloud line A – A' indicates convergence with thick convective clouds (known as the Sea of Japan Polar Air Mass Convergence Zone, or JPCZ), which often brings heavy snow in winter. The lower winter version provides high contrast between developed ice clouds and water clouds.

contribution from Band 4. Hotspots relating to fire appear in cyan. High brightness temperatures in Bands 13 and 7 radiance cause this color in RGB imagery.

As color display in mid-to-high latitude areas is not applicable to winter, a winter version of Day Microphysics RGB is offered (Table 2) with adjusted thresholds for green beam Band 7 (Fig.

12). The winter version offers high contrast between clouds in such cases.

As shown in Table 9, various color indications and related interpretations apply with Day Microphysics RGB, allowing detailed clarification of clouds and surface situations. However, user familiarity with this RGB (e.g., expertise in the physical characteristics of the three band components) may be required for appropriate and efficient usage.

3.5. Day Convective Storm RGB (Day Convection RGB)

Day Convective Storm (also known as Day Convection) RGB is ideal for identifying convective cloud with strong updrafts during the daytime. The RGB scheme was originally designed for MSG operation by EUMETSAT, and is non-standard among WMO schemes. However, it is considered useful and is widely applied in various regions other than MSG observation areas.

Day Convective Storm RGB involves the assignment of red/green/blue to difference imagery for Band 10 ($7.3 \mu\text{m}$) – Band 8 ($6.2 \mu\text{m}$), Band 13 ($10.4 \mu\text{m}$) – Band 7 ($3.9 \mu\text{m}$) and Band 3 ($0.64 \mu\text{m}$) – Band 5 ($1.6 \mu\text{m}$) (Table 10).

The temperature difference of Band 10 – Band 8 ($\text{BTD}_{\text{B10-B08}}$) in the red beam highlights thick high clouds. Heavy clouds such as the Cb type exhibit low or almost-zero values in $\text{BTD}_{\text{B10-B08}}$ imagery. Band 13 – Band 7 ($\text{BTD}_{\text{B13-B07}}$) in the green beam highlights strong convective updrafts with small ice particles. Due to the significant contribution from Band 7's solar reflection for small ice particles in the daytime, $\text{BTD}_{\text{B13-B07}}$ values tend to be high. The reflectivity difference of Band 3 – Band 5 ($\text{RD}_{\text{B03-B05}}$) in the blue beam emphasizes the contrast between ice clouds and other types. Ice clouds in forms such as cirrus and developed Cb show negative values in $\text{RD}_{\text{B03-B05}}$ imagery.

Table 10: Band components and related specifications for Day Convective Storm RGB

Color	AHI Bands	Central wave length [μm]	Physically relates to	Smaller contribution to the signal of	Larger contribution to the signal of
Red	B10-B08	7.3-6.2	Cloudtop height	Low level clouds	High level clouds
Green	B13-B07	10.4-3.9	Cloud top particle size and temperature	Large ice particles with weak updrafts	Small ice particles with strong updrafts
Blue	B03-B05	0.64-1.6	Cloud top phase	Ice clouds	Water clouds

Table 11: Color interpretation and RGB values for Day Convective Storm RGB

Color	Interpretation	RGB Value	HTML
	Deep precipitating cloud (precip. not necessarily reaching the ground) - high-level cloud, large ice particles	225,38,14	#E1260E
	Deep precipitating cloud (Cb cloud with strong updrafts and severe weather)* - high-level cloud, small ice particles *or thick, high-level lee cloudiness with small ice particles	255,255,100	#FFFF64
	Thin Cirrus cloud (large ice particles)	170,40,90	#AA285A
	Thin Cirrus cloud (small ice particles)	170,60,175	#AA3CAF
	Ocean	60,0,170	#3C00AA
	Land	86,6,255	#5606FF

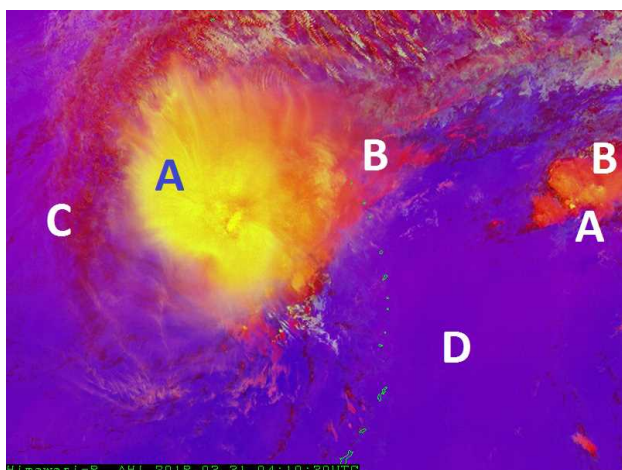


Fig. 13: Typhoon Jelawat (T1803) around the Mariana Islands (0410 UTC, 31 March 2018)
 A: Cb cloud with strong updrafts or high-level cloud with small ice particles; B: thick high-level cloud with large ice particles; C: thin cirrus cloud; D: sea surface

Color interpretation for Day Convective Storm RGB is shown in Table 11. Thick clouds appear red due to high contribution from the red beam of $\text{BTD}_{\text{B10-B08}}$. Cb clouds with strong updraft appear yellowish. Strong updrafts in Cb clouds carry small ice particles to the cloud top before

cloud particles grow larger (Fig. 13). Such thick cloud tops show high contributions from $\text{BTD}_{\text{B13-B07}}$ and $\text{BTD}_{\text{B10-B08}}$ as well as low contributions from $\text{RD}_{\text{B03-B05}}$ (with the combination of red and green producing yellow).

In this way, Day Convective Storm RGB is useful in the monitoring of heavy convective cloud coverage in the daytime. However, it is unsuitable for distinguishing low-level cloud.

3.6. Night Microphysics RGB

Night Microphysics RGB is a specific scheme for nighttime (i.e., for application when no solar radiation is present). It is particularly useful for the important task of distinguishing fog and low cloud from cloud-free areas at nighttime for traffic security.

Table 12 shows the formation of red/green/blue beams assigned to the product.

The difference imagery of Band 13 ($10.4 \mu\text{m}$) – Band 15 ($12.4 \mu\text{m}$) ($\text{BTD}_{\text{B13-B15}}$) assigned to the red beam of the RGB helps users to distinguish between thick and thin clouds. Thick clouds show almost-zero values and thin clouds show

Table 12: Band components and related specifications for Night Microphysics RGB

Color	AHI Bands	Central wave length [μm]	Physically relates to	Smaller contribution to the signal of	Larger contribution to the signal of
Red	B13-B15	10.4-12.4	Cloud optical thickness	Thin clouds	Thick clouds
Green	B07-B13	3.9-10.4	Cloud phase	Thin ice clouds	Thick fog/ water clouds
Blue	B13 (inverse)	10.4	Cloud top temperature Temperature of surface	Cold clouds Cold surface	Warm clouds Warm surface

Table 13: Color interpretation and RGB values for Night Microphysics RGB

Color	Interpretation	RGB Value	HTML
	Cold, thick, high-level cloud	140,10,0	#8C0A00
	Very cold, thick, high-level cloud	-	-
	Thin Cirrus cloud	0,0,60	#00003C
	Thick, mid-level cloud	140,120,70	#8C7846
	Thin, mid-level cloud	0,120,90	#00785A
	Low-level cloud (cold atmosphere, High latitude)	200,250,170	#C8FAAA
	Low-level cloud (warm atmosphere, low latitude)	170,200,230	#AAC8E6
	Ocean	123,128,233	#7B80E9
	Land	192,100,165	#C064A5

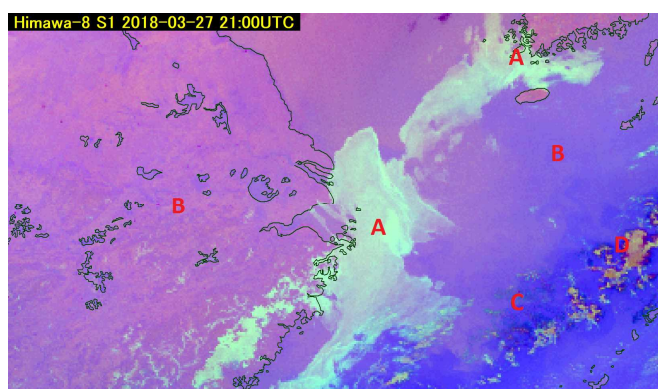


Fig. 14: Fog/low-level cloud around the East China Sea and the Yellow Sea (2100 UTC, 27 March 2018)

A: fog/low-level cloud; B: land and ocean (cloud-free); C: thin cirrus cloud; D: thick mid-level cloud

positive values in $\text{BTD}_{\text{B13-B15}}$ imagery. With the green beam, difference imagery of Band 7 ($3.9 \mu\text{m}$) – Band 13 ($\text{BTD}_{\text{B07-B13}}$) is effective for detecting fog/low cloud (water cloud). As the emissivity of Band 7 is much lower than that of

Band 13 for thick water cloud, the relevant $\text{BTD}_{\text{B07-B13}}$ is negative. Band 13 assigned to the blue beam provides information on surface and cloud top temperatures. As with the blue beam in Day Microphysics RGB, this consists of inverted IR imagery (with warm pixels contributing blue to RGB imagery).

Color interpretation for Night Microphysics RGB is shown in Table 13. Low-level water clouds appear bright greenish/bluish due to high contributions from all color beams, especially the green of $\text{BTD}_{\text{B07-B13}}$ and the blue of Band 13. As the contribution from the blue beam from Band 13 depends on thermal conditions such as latitude and season, water clouds appear bluish in warmer environments due to higher contribution from the blue beam (Fig. 14). Thick clouds such as the Cb type appear reddish due to high contribution from the red beam from $\text{BTD}_{\text{B13-B15}}$. For very cold (around 220 K) thick cloud areas such as Cb tops, contribution from the green beam of $\text{BTD}_{\text{B07-B13}}$ is added. However,

as Band 7 shows discrete values at very low temperatures, very cold thick clouds appear reddish or orange with yellow scattering (“A” in Fig. 15). Thin high clouds appear dark due to lower contributions from all beams.

Colors of surface areas (i.e., land and sea) are affected by thermal conditions as well as low-level cloud. Sea areas generally appear bluish, while the colors of land (especially inland areas) depend on the diurnal variation of surface temperature (“B” in Fig. 14 and “F” in Fig. 15).

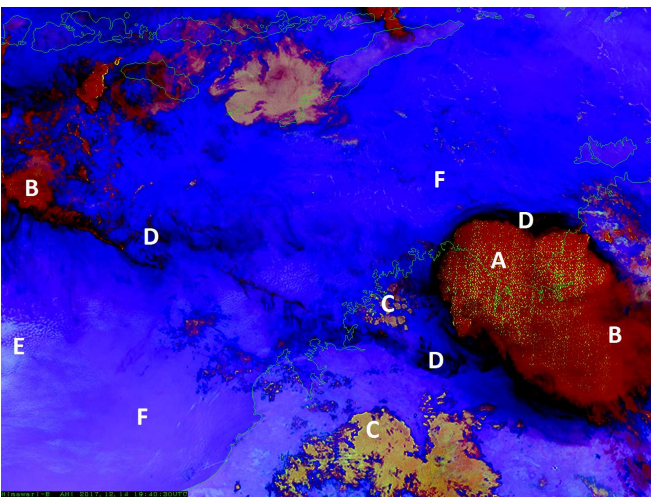


Fig. 15: Cb clouds around Northwestern Australia (1940 UTC, 14 December 2017)

A: Cb cloud with thick, very cold top; B: thick cloud with cold top; C: thick mid-level cloud; D: thin cirrus cloud; E: low-level warm cloud; F: sea surface

3.7. 24-hour Microphysics RGB schemes

The 24-hour Microphysics RGB (cloud), Dust RGB and Ash RGB products all share a color scheme. To allow specialization of individual applications for cloud analysis, Aeolian dust detection and volcanic ash and gas detection, related thresholds (temperature ranges and gamma values) are adjusted.

The advantage of this scheme is its appropriacy irrespective of time, with RGBs applicable day

and night throughout the year thanks to their constitution based only on IR (mid-long wave length IR) observation bands. WMO’s RGB workshop considers such RGBs to be highly robust for operational weather monitoring while also recognizing the value of blended products (WMO 2007, 2012).

These RGBs are composed of red/green/blue assigned to difference imagery of Band 13 (10.4 μm) – Band 15 (12.4 μm) ($\text{BTD}_{\text{B13-B15}}$), Band 11 (8.6 μm) – Band 13 (10.4 μm) ($\text{BTD}_{\text{B11-B13}}$)/Band 11 (8.6 μm) – Band 14 (11.2 μm) ($\text{BTD}_{\text{B11-B14}}$) and Band 13 (Table 14, as an example of 24-hour microphysics RGB (cloud)). For the green beam, there are two appropriate combinations in comparison with MSG Channel 9 (10.8 μm) – Channel 7 (8.7 μm). Related difference images support identification of cloud phase, dust and volcanic gas (SO_2). The red beam of $\text{BTD}_{\text{B13-B15}}$ is effective for detecting dust and volcanic ash and for distinguishing between thick and thin clouds. The blue beam of Band 13 provides information on surface and cloud top temperatures. Contributions from the respective color beams for these RGBs are detailed below.

3.7.1 24-hour Microphysics RGB (Cloud)

The 24-hour Microphysics RGB (cloud) product has specific thresholds for cloud analysis performed during daytime and nighttime. This type of RGB is frequently referred to simply as “24-hour Microphysics RGB” with the “(Cloud)” part omitted.

The $\text{BTD}_{\text{B13-B15}}$ range assigned to the red beam of the RGB helps users to distinguish between thick and thin clouds (cloud optical thickness) in conjunction with the Night Microphysics RGB scheme (Table 14). Thick clouds show almost-zero values and thin clouds show positive values in $\text{BTD}_{\text{B13-B15}}$ imagery. The $\text{BTD}_{\text{B11-B13}}$ / $\text{BTD}_{\text{B11-B14}}$ ranges assigned to the RGB green beam are helpful for distinguishing between water clouds

Table 14: Band components and related specifications for 24-hour Microphysics RGB (cloud)

Color	AHI Bands	Central wave length [μm]	Physically relates to	Smaller contribution to the signal of	Larger contribution to the signal of
Red	B13-B15	10.4-12.4	Cloud optical thickness	Thin ice clouds	Thick clouds
Green	B11-B13 /B11-B14	8.6-10.4 /8.6-11.2	Cloud phase	Ice clouds	Water clouds
Blue	B13 (inverse)	10.4	Cloud top temperature Temperature of surface	Cold clouds Cold surface	Warm clouds Warm surface

Table 15: Color interpretation and RGB values for 24-hour Microphysics RGB (cloud)

Color	Interpretation	RGB Value	HTML
	Thick, high and cold ice clouds	147,0,0	#930000
	Thick water clouds	157,99,40	#9D6328
	Clouds with small particles	32,180,125	#20B47D
	Thin cirrus clouds	0,0,0	#000000
	Dust (Yellow sand)	255,0,146	#FF0092
	Sands with quartz mineral	207,239,239	#CFEFEF

and ice clouds, with the former showing larger positive values and the latter showing smaller values. The contrast of $BTD_{B11-B14}$ difference values for water/ice clouds is higher than that of $BTD_{B11-B13}$. Accordingly, $BTD_{B11-B14}$ appears superior as the green band for 24-hour microphysics RGB (cloud) in consideration of its primary aim. The blue beam of Band 13 provides information on surface and cloud top temperatures (with warm pixels contributing blue to RGB imagery) in addition to Day and Night Microphysics RGB.

Color interpretation for 24-hour Microphysics RGB is shown in Table 15 (Lensky and Rosenfeld 2008). Thick clouds with ice crystals (such as Cb) appear dark reddish due to medium/high contribution from the red beam of $BTD_{B13-B15}$ and low contributions from the green beam of $BTD_{B11-B13}/BTD_{B11-B14}$ and the blue beam of Band 13. Thick water clouds appear ocher due to medium contributions from the red beam of $BTD_{B15-B13}$ and the green beam of $BTD_{B11-B13}/BTD_{B11-B14}$. Thin Ci clouds appear deep black due to low contributions from all color beams. Notably, dust and volcanic ash appear pinkish or magenta in this RGB representation (see the Dust RGB and Ash RGB sections for details). Figure

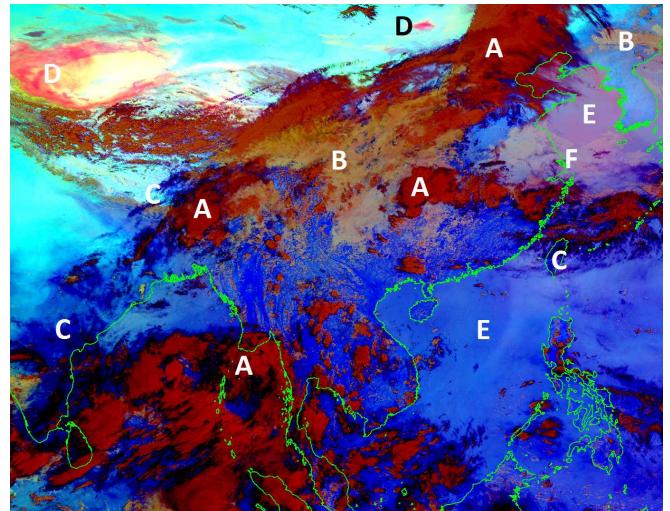


Fig. 16: Various clouds and desert areas around Southeast Asia, China, India and the surrounding region with green beam: $BTD_{B11-B14}$ version (0600 UTC, 26 May 2018)

A: thick cloud with large ice particles; B: thick cloud with small ice particles (including Cb cloud with strong updrafts); C: thick water cloud with super-cooled small droplets; D: thick water cloud with large droplets; E: thin water cloud with super-cooled small droplets; F: high-level lee cloudiness with small ice particles; G: thin cirrus cloud; H: sea surface

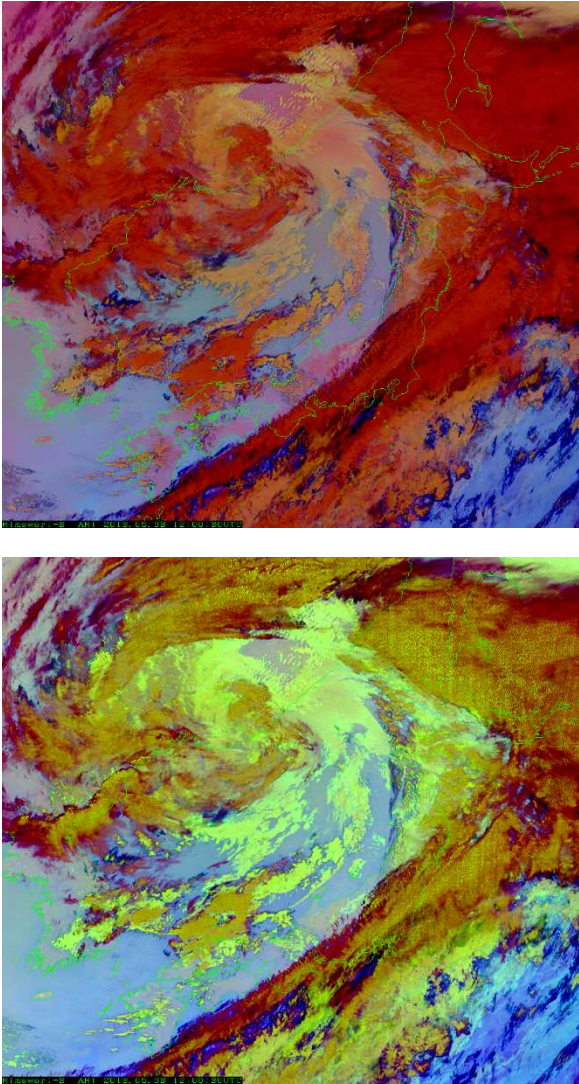


Fig. 17: Comparison between 24-hour Microphysics RGB with green beam: $BTD_{B11-B14}$ version (top) and Night Microphysics RGB (bottom) (1200 UTC, 3 May 2018)

16 shows an example of 24-hour microphysics RGB interpretation including color interpretations in addition to those of Table 15 (with extra input based on subsequent studies). The color shading in the left part (western area) of the image is affected by the infrared-band limb cooling effect caused by increased atmospheric absorption between the satellite and the earth depending on the viewing angle.

Figure 17 compares 24-hour Microphysics RGB and Night Microphysics RGB. The latter is

generally superior for nighttime discrimination of low-level and other types of cloud, while the former is applicable for both daytime and nighttime analysis. These RGBs need to be used appropriately in line with user goals.

3.7.2 Dust RGB

Dust RGB has specific thresholds for daytime and nighttime Aeolian dust detection. It can also be used to identify thin cirrus clouds and distinguish water clouds from thick ice clouds as with 24-hour Microphysics RGB (Cloud).

The $BTD_{B13-B15}$ range assigned to the red beam of the RGB helps users to distinguish between thick and thin clouds (cloud optical thickness) as with 24-hour Microphysics RGB (Cloud) (Table 16). Thick clouds show almost-zero values and thin clouds show positive values in $BTD_{B13-B15}$ imagery. For dust and volcanic ash in the atmosphere, signals from $BTD_{B13-B15}$ have negative values. The $BTD_{B11-B13}/BTD_{B11-B14}$ ranges assigned to the green beam of the RGB are useful in distinguishing between water clouds and ice clouds, as with 24-hour Microphysics RGB (Cloud). Water clouds show larger positive values and ice clouds show smaller values in $BTD_{B11-B13}/BTD_{B11-B14}$ imagery, while dust and volcanic ash show larger positive values. The contrast of $BTD_{B11-B13}$ difference values for water/ice clouds is generally superior, but this does not necessarily apply to dust and ash due to differences in emission from land and sea immediately below affected areas. $BTD_{B11-B13}$ appears to be empirically better for dust drifting over such areas (Fig. 18). The blue beam of Band 13 provides information on surface and cloud top temperatures (with warm pixels contributing blue to RGB imagery) as with Day and Night Microphysics RGB.

The color interpretation for Dust RGB shown in Table 17 is similar to that for 24-hour

Table 16: Band components and related specifications for Dust RGB

Color	AHI Bands	Central wave length [μm]	Physically relates to	Smaller contribution to the signal of	Larger contribution to the signal of
Red	B13-B15	10.4-12.4	Cloud optical thickness Dust	Thin ice clouds	Thick clouds Dust
Green	B11-B13 /B11-B14	8.6-10.4 /8.6-11.2	Cloud phase	Thin ice clouds Dust	Water clouds Deserts
Blue	B13 (inverse)	10.4	Cloud top temperature Temperature of surface	Cold clouds Cold surface	Warm clouds Warm surface

Table 17: Color interpretation and RGB values for Dust RGB

Color	Interpretation	RGB Value	HTML
	Cold, thick, high-level clouds	140,0,0	#8C0000
	Thin Cirrus clouds Contrails	0,0,0	#000000
	Thick, mid-level cloud	160,110,50	#A06E32
	Thin, mid-level cloud	40,121,80	#287950
	Low-level cloud (cold atmosphere, High latitude)	189,176,1	#BDB001
	Low-level cloud (warm atmosphere, low latitude)	183,95,218	#B75FDA
	Dust (Yellow sand)/ Volcanic ash	255,96,202	#FF60CA
	Ocean	130,130,190	#8282BE
	Warm desert	170,240,255	#AAF0FF
	Cold desert	170,240,140	#AAF08C
	Warm land	150,150,255	#9696FF
	Cold land	160,98,126	#A0627E

Microphysics RGB (cloud), and colors for cloud analysis have been added from subsequent research.

Dust (or volcanic ash) appears bright magenta or pinkish due to high contributions from the red beam of $BTD_{B13-B15}$ and the blue beam of Band 13, and medium contribution from the green beam of $BTD_{B11-B13}/BTD_{B11-B14}$. The contribution from Band 13 depends on the temperature of dust clouds and the underlying surface.

Thick clouds with ice crystals, such as Cb, appear dark reddish due to medium contribution from the red beam of $BTD_{B13-B15}$ and low contributions from the green beam of $BTD_{B11-B13}/BTD_{B11-B14}$ and the blue beam of Band 13. Thin Ci clouds appear deep black due to low contributions from all color beams. Thick mid-

level clouds appear other due to medium contributions from the red beam of $BTD_{B13-B15}$ and the green beam of $BTD_{B11-B13}/BTD_{B11-B14}$. Thin mid-level clouds appear dark greenish due to medium contributions from the green beam of $BTD_{B11-B13}/BTD_{B11-B14}$. The main colors for low-level clouds depend on surrounding thermal conditions (e.g., temperature, latitude and season). Warmer low-level clouds appear purplish due to medium to high contributions from the red beam of $BTD_{B13-B15}$ and the blue beam of Band 13. Colder low-level clouds appear dark yellowish due to medium contributions from the red beam of $BTD_{B13-B15}$ and the green beam of $BTD_{B11-B13}/BTD_{B11-B14}$.

Colors for land and desert areas depend on thermal conditions. Comparison of daytime and

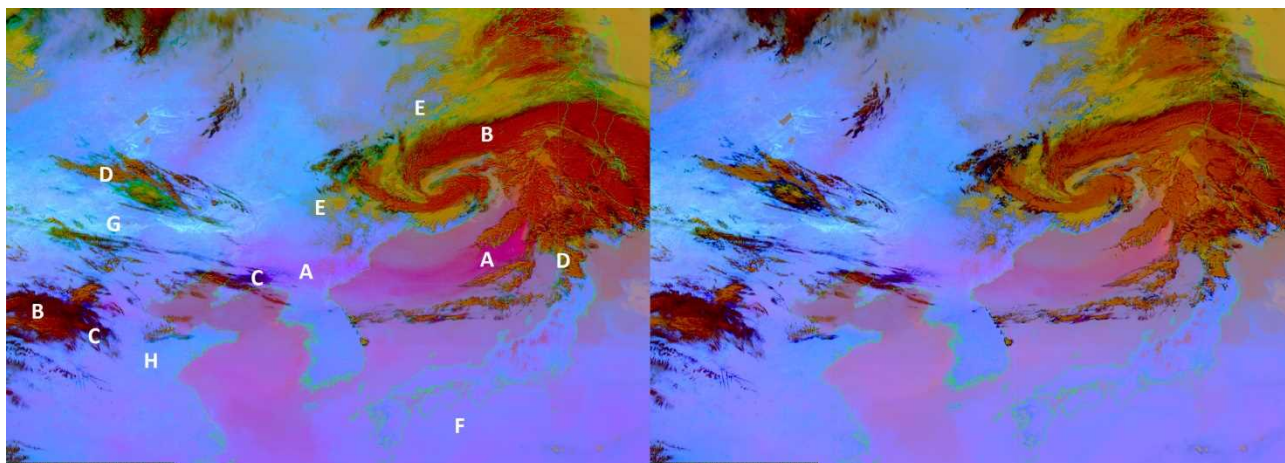


Fig. 18: Comparison of Asian dust around East Asia between Dust RGB with green beam: $BTD_{B11-B13}$ version (left) and Dust RGB with green beam: $BTD_{B11-B14}$ version (right) (0120 UTC, 30 April 2017). Dust distributed over sea areas is clearer in Dust RGB with green beam: $BTD_{B11-B13}$ version in this case.

A – A: dust; B: thick high-level cloud; C: thin cirrus cloud; D: thick mid-level cloud; E: low-level cloud; F: sea surface; G: warm desert; H: warm land

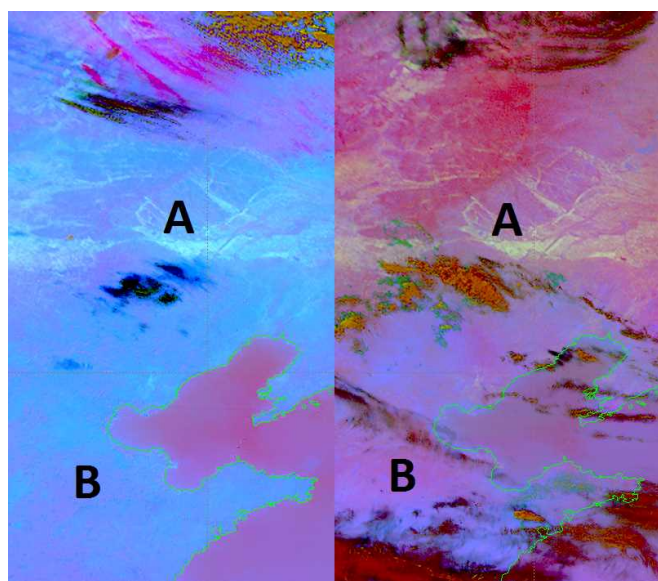


Fig. 19: Difference of surface color shade between daytime (left: 0300 UTC) and nighttime (right: 1200 UTC) (both for 30 April 2017)

A: desert (left: warm/right: cold); B: land (left: warm/right: cold)

nighttime image highlights diurnal changes via these colors (Fig. 19). Diurnal and seasonal changes can also be seen in other RGB imagery incorporating infrared bands, such as 24-hour

Microphysics RGB (cloud) and Night Microphysics RGB. Warm desert areas appear bright bluish due to high contributions from all color beams, especially the green beam of $BTD_{B11-B13}/BTD_{B11-B14}$ and the blue beam of Band 13. Cold land appears dark purplish due to primarily medium contributions from the red beam of $BTD_{B13-B15}$ and the blue beam of Band 13.

Dust RGB is thus useful for distinguishing dust clouds in daytime and nighttime observation, but does not provide quantitative information on dust cloud concentration. As dust clouds may be unclear in Dust RGB imagery depending on states of concentration and underlying surfaces, care is required in dust detection.

3.7.3 Ash (Volcanic Ash) RGB

Ash RGB has specific thresholds for volcanic ash and gas (sulfur dioxide: SO_2) detection during daytime and nighttime.

The $BTD_{B13-B15}$ range assigned to the red beam of the RGB supports the detection of volcanic ash clouds in the atmosphere. Signals from $BTD_{B13-B15}$ have negative values for ash clouds, and the

Table 18: Band components and related specifications for Ash RGB

Color	AHI Bands	Central wave length [μm]	Physically relates to	Smaller contribution to the signal of	Larger contribution to the signal of
Red	B13-B15	10.4-12.4	Cloud optical thickness Volcanic ash	Thin ice clouds	Thick clouds Volcanic ash
Green	B11-B13 /B11-B14	8.6-10.4 /8.6-11.2	Cloud phase	Thin ice clouds Volcanic ash	Water clouds SO ₂ gas plume
Blue	B13 (inverse)	10.4	Cloud top temperature Temperature of surface	Cold clouds Cold surface	Warm clouds Warm surface

Table 19: Color interpretation and RGB values for Ash RGB

Color	Interpretation	RGB Value	HTML
	Cold, thick, high-level clouds	158,86,5	#9E5605
	Thin Cirrus clouds Contrails	15,10,4	#0F0A04
	SO ₂ gas plume (shades of bright green depending on the concentration)	87,255,188	#57FFBC
	Volcanic ash (shades of red depending on the concentration)	230,9,3	#E60903

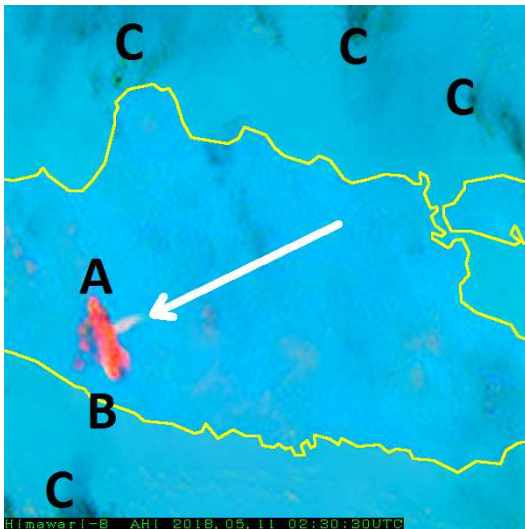


Fig. 20: Eruption of Mt. Merapi, Indonesia (0230 UTC, 11 May 2018). The white arrow indicates a volcanic plume.

A: volcanic ash; B: volcanic ash with SO₂ gas (yellowish pixels); C: thin cirrus cloud

red beam of this RGB is useful in distinguishing thick and thin clouds (cloud optical thickness) as with 24-hour Microphysics RGB (cloud) and Dust RGB (Table 18). Thick clouds exhibit almost-zero values and thin clouds exhibit positive values in $\text{BTD}_{\text{B13-B15}}$ imagery. The $\text{BTD}_{\text{B11-B13}}/\text{BTD}_{\text{B11-B14}}$ range assigned to the green beam of the RGB is useful in

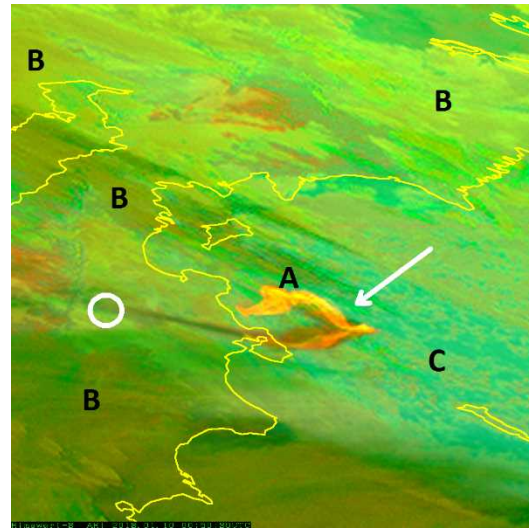


Fig. 21: Eruption of Mt. Shiveluch, Russia (0050 UTC, 10 January 2018). The white circle and arrow indicate Mt. Shiveluch and its volcanic plume.

A: volcanic ash with SO₂ gas; B: thick mid/high-level cloud; C: low/mid-level cloud

distinguishing between water clouds and ice clouds as with 24-hour Microphysics RGB (cloud) and Dust RGB. SO₂ is also detectable due to absorption in Band 11. As with 24-hour Microphysics RGB and other RGBs, Band 13 assigned to the blue beam consists of inverted IR

imagery (with warm pixels contributing blue to RGB imagery). The color interpretation for Ash RGB shown in Table 19 illustrates the characteristic hues used for volcanic plumes. These largely depend on viewing angle, concentration, transparency, temperature, surface emissivity and water vapor content as with 24-hour Microphysics RGB.

Volcanic ash appears reddish or pinkish due to high contributions from the red beam of $BTD_{B13-B15}$, with additional variation depending on ash concentration. SO_2 gas plumes appear bright greenish due to high contribution from the green beam of $BTD_{B11-B13}/BTD_{B11-B14}$, with additional variation depending on SO_2 concentration. Volcanic ash is often accompanied by the presence of gas, and appears yellowish in combination with SO_2 due to high contributions from red and green beam content.

Thick (high) ice clouds appear brown due to medium contributions from the red beam of $BTD_{B13-B15}$ and the green beam of $BTD_{B11-B13}/BTD_{B11-B14}$. Thick volcanic ash is also known to appear in this color. Thin ice clouds appear dark bluish due to low contributions from all three beams. The shade of blue depends on cloud transparency.

Ash RGB supports monitoring of volcanic ash and gas, but the presence of ice particles (e.g., in cirrus cloud mixed with volcanic plume content) can hinder the interpretation of display colors.

Figure 20 illustrates the tropical (warm) atmosphere eruption of Mt. Merapi as per the True Color RGB in Fig. 9. The yellowish pixels seen in the reddish ash plume represent ash mixed with volcanic SO_2 gas (i.e., red and green beam contributions).

Figure 21 shows high-latitude (cold) atmosphere effects from the eruption of Mt. Shiveluch, with greenish coloring as compared to low-latitude (tropical) representation. The volcanic plume (marked “A”) appears to contain

volcanic SO_2 gas as with Mt. Merapi.

3.8. Airmass RGB

Airmass RGB is useful for analyzing air masses and descending dry stratospheric air associated with jet streams and potential vorticity (PV) anomalies in synoptic systems (Fig. 22).

This RGB is composed of red/green/blue assigned to difference imagery for Band 10 ($7.3 \mu\text{m}$) – Band 8 ($6.2 \mu\text{m}$) ($BTD_{B10-B08}$), Band 13 ($10.4 \mu\text{m}$) – Band 12 ($9.6 \mu\text{m}$) ($BTD_{B13-B12}$) and the single imagery of Band 8 (Table 20). Thus, Airmass RGB incorporates two water vapor bands (Bands 8 and 10) and the ozone absorption band (Band 12). Table 20 shows the formation of red/green/blue beams assigned to this RGB.

The temperature difference in $BTD_{B10-B08}$ for the red beam indicates vertical (mid/high-level) water vapor distribution. Dry atmospheric conditions are characterized by low values (with high contribution for the red beam), and moist atmospheric conditions in the mid-level range exhibit high values in $BTD_{B10-B08}$ imagery. This also highlights thick high clouds as with the red beam in Day Convective Storm RGB. High clouds and thick clouds (e.g., Cb) exhibit low or almost-zero values. $BTD_{B13-B12}$ for the green beam indicates tropopause height based on atmospheric ozone amounts. Such ozone is mainly produced in the stratosphere over tropical regions and transported to higher latitudes via Brewer-Dobson circulation, and is prevalent in cold air masses due to conditions involving a low tropopause with a thick ozone-rich stratosphere. Such polar air masses exhibit large positive values (with low contribution for the green beam, manifesting as darker in imagery), while less-dense ozone tropical air masses exhibit smaller values (with high contribution for the green beam, manifesting as brighter in imagery).

Clouds are seen in $BTD_{B13-B12}$, and thick Cb clouds exhibit particularly large negative values

Table 20: Band components and related specifications for Airmass RGB

Color	AHI Bands	Central wave length [μm]	Physically relates to	Smaller contribution to the signal of	Larger contribution to the signal of
Red	B10-B08	7.3-6.2	Vertical water vapor distribution Mid-high level clouds	Mid-level humidity Mid-level clouds	Dry upper levels High-level clouds
Green	B13-B12	10.4-9.6	Tropopause height based on ozone Clouds at all levels	Low tropopause (Polar Air mass) with ozone rich	High tropopause (Tropical Air mass) with ozone poor
Blue	B08	6.2	Water vapor distribution at upper level High clouds	Dry upper levels Warm brightness temperatures	Moist upper levels Cold brightness temperatures

Table 21: Color interpretation and RGB values for Airmass RGB

Color	Interpretation	RGB Value	HTML
	Thick, high-level clouds	255,255,255	#FFFFFF
	Thick, mid-level clouds	240,190,160	#F0BEA0
	Thick, low-level clouds (warm airmass)	47,107,40	#2F6B28
	Thick, low-level clouds (cold airmass)	73,70,115	#494673
	Jet (high PV, descending dry stratospheric air)	131,8,12	#83080C
	Cold air mass	58,8,126	#3A087E
	Warm air mass (high upper tropospheric humidity)	27,114,32	#1B7220
	Warm air mass (low upper tropospheric humidity)	114,114,0	#727200

(with high contribution for the green beam). Band 8 of the blue beam supports the visualization of water vapor distribution in the upper troposphere as with water vapor imagery. Upper-level moisture and high-level clouds indicate lower temperatures (with high contribution for the blue beam).

Color interpretation for Airmass RGB is shown in Table 21. Warm air masses in the mid-upper troposphere appear greenish due to primarily medium contribution from the green beam of $\text{BTD}_{\text{B13-B12}}$. Greenish shading depends on upper-level moisture (with warm air masses in dry upper-troposphere conditions appearing olive due to medium contribution from the red beam of $\text{BTD}_{\text{B10-B08}}$), and cold air masses appear dark purplish due to primarily medium contribution from the blue beam of Band 8. Dry descending stratospheric air, high PV (potential vorticity) originating in the stratosphere and jet streams in dry air masses appear dark reddish (Fig. 23) due to medium contribution from the red beam of

$\text{BTD}_{\text{B10-B08}}$ (suggesting dry upper air) and low contributions from the green beam of $\text{BTD}_{\text{B13-B12}}$ and the blue beam of Band 8 (suggesting lower tropopause height with rich ozone and dry upper air, respectively). Thick high-level clouds appear bright whitish due to high contributions from all color beams.

In addition, Band 10, which forms the $\text{BTD}_{\text{B10-B08}}$ of the red beam, is sensitive to SO_2 gas. As a result, volcanic SO_2 plumes in the mid-level troposphere appear reddish (Fig. 24).

This RGB is suitable for analysis of synoptic-scale systems. However, greater absorption at larger satellite viewing angles causes false blue/violet representation along the entire limb of full-disk images. This is a result of cooler brightness temperature relating to absorption, known as the limb cooling effect (Fig. 22).

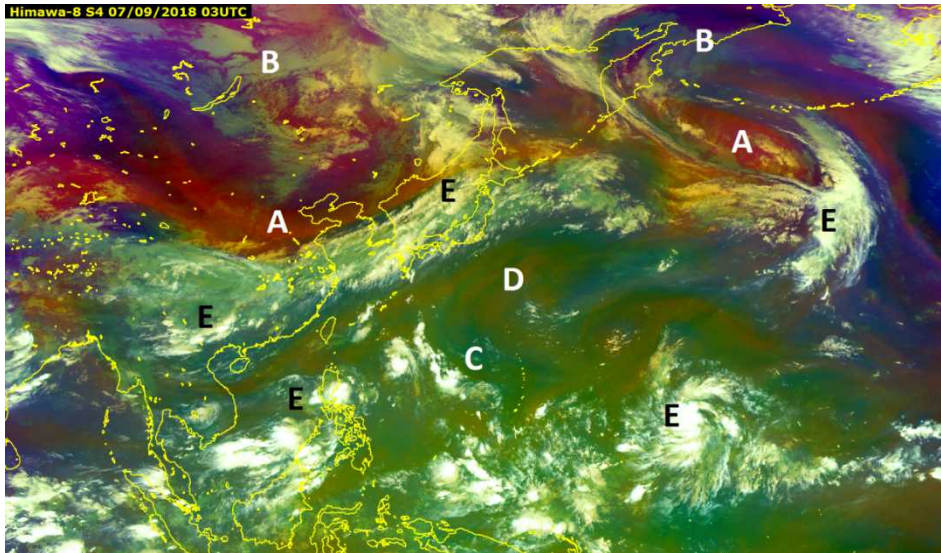


Fig. 22: Example of Airmass RGB imagery and related interpretation (0300 UTC, 7 September 2018)

A: jet stream (left); high PV area with descending dry stratospheric air (right); B: cold (ozone-rich) air mass; C: warm (ozone-poor) air mass (high upper tropospheric humidity); D: warm (ozone-poor) air mass (low upper tropospheric humidity); E: high-level thick cloud

The left (western) part of the image is affected by limb cooling as seen in Fig. 16 (24-hour Microphysics RGB).

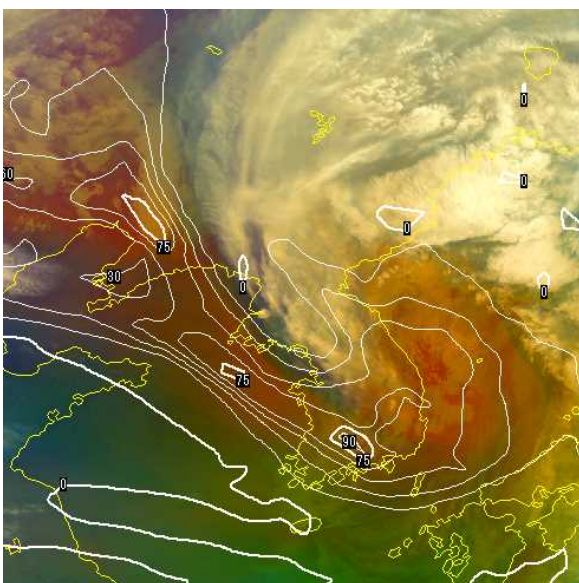


Fig. 23: A developing low around the Korean Peninsula. White lines indicate PV (0.1 PV units) at 300 hPa based on numerical weather prediction displayed over Airmass RGB imagery (2100 UTC, 16 April 2016).

The reddish area shows favorable correspondence to the high PV area.

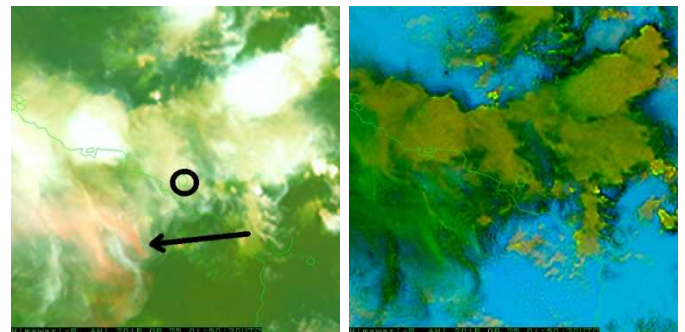


Fig. 24: Eruption comparison (Mt. Manam, Papua New Guinea) between Airmass RGB (top) and Ash RGB with green beam: BTDB11-B14 version (bottom) (0150 UTC, 25 August 2018)

The black circle and arrow indicate Mt. Manam and a volcanic plume with SO₂ gas (reddish area), respectively.

New RGB composite and other useful composite schemes

As detailed in the previous section, the widely used RGB composite schemes based on MSG operation by EUMETSAT are also useful to Himawari-8 users. Useful RGB schemes for low-earth orbit (LEO) meteorological satellites

Table 22: New RGB and other useful RGB composites with recommended thresholds for Himawari-8

	H8 Bands	Central wave	Min [K/%]	Max [K/%]	Gamma
Simple water vapor RGB					
R	B13	10.4	202.3K	279.0K	10.0
G	B08	6.2	214.7K	242.7K	5.5
B	B10	7.3	245.1K	261.0K	5.5
Differential water vapor RGB					
R	B10-B08	7.3-6.2	-3.0K	30.0K	3.5
G	B10	7.3	213.2K	278.2K	2.5
B	B08	6.2	208.5K	243.9K	2.5
Cloud phase distinction RGB					
R	B13	10.4	219.6K	280.7K	1.0
G	B03	0.64	0%	85%	1.0
B	B05	1.6	1%	50%	1.0
Day cloud phase RGB					
R	B05	1.6	0%	50%	1.0
G	B06	2.3	0%	50%	1.0
B	B01	0.47	0%	100%	1.0
Day deep clouds RGB					
R	B13-B08	10.4-6.2	-5.0K	35.0K	1.0
G	B03	0.64	70%	100%	1.0
B	B13 (inverse)	10.4	243.6K	292.6K	1.0
Natural fire color RGB					
R	B06	2.3	0%	100%	1.0
G	B04	0.86	0%	100%	1.0
B	B03	0.64	0%	100%	1.0
Fire temperature RGB					
R	B07	3.9	273.0K	350.0K	1.0
G	B06	2.3	0%	50%	1.0
B	B05	1.6	0%	50%	1.0
SO2 RGB					
R	B10-B09	7.3-6.9	-6.0K	5.0K	1.0
G	B11-B13 /B11-B14	8.6-10.4 /8.6-11.2	-1.6K -5.9K	4.9K 5.1K	1.2 0.85
B	B13 (inverse)	10.4	243.6K	303.2K	1.0

imagery include those of the NOAA series operated by the USA's National Oceanic and Atmospheric Administration (NOAA) in addition to those described above (NASA SPoRT, 2017-2018).

As the new-generation AHI/Himawari-8 geostationary earth orbit (GEO) satellite has its own observation bands (such as Band 6 (2.3 μm) and Band 9 (6.9 μm)), new and alternative useful RGB schemes are required for the effective usage of Himawari imagery (Shimizu, 2017).

Table 22 lists new RGB and other useful RGB composites, along with recommended thresholds for Himawari-8. The thresholds remain under consideration, and may be improved in the future. The individual schemes are detailed below.

4.1. Simple Water Vapor RGB

JMA's Simple Water Vapor RGB enables analysis of water vapor distribution for individual levels excluding cloud areas. Composed of the red/green/blue assigned to the imagery of Band 13 (10.4 μm), Band 8 (6.2 μm) and Band 10 (7.3 μm) (Table 23), this scheme can be used for simultaneous daytime and nighttime analysis of low/mid-level cloud (Band 13), mid-level cloud (Band 10), high-level cloud (Band 8) and water vapor distribution. Low-level cloud may not be visible in some cases due to gamma-value stretching.

Color interpretation for Simple Water Vapor RGB is shown in Table 24. Clouds with a high-level top appear bright whitish due to high contributions from all color beams, while dry and cloudless areas appear black due to low contributions from all color beams. Low/mid-level clouds with dry atmospheric conditions appear red or dark reddish due to medium/high contribution from the red beam of Band 13, while mid-level clouds with humid atmospheric conditions at low/mid-levels appear magenta due to high contributions from the red beam of Band

Table 23: Band components and related specifications for Simple Water Vapor RGB

Color	AHI Bands	Central wave length [μm]	Physically relates to	Smaller contribution to the signal of	Larger contribution to the signal of
Red	B13	10.4	Cloud top temperature	Warm clouds	Cold clouds
Green	B08	6.2	Water vapor distribution at upper level	Dry upper levels Warm brightness temperatures	Moist upper levels Cold brightness temperatures
Blue	B10	7.3	Water vapor distribution at Mid-level	Dry Mid-levels Warm brightness temperatures	Moist Mid-levels Cold brightness temperatures

Table 24: Color interpretation and RGB values for Simple Water Vapor RGB

Color	Interpretation	RGB Value	HTML
	Clouds with high level top	255,255,255	#FFFFFF
Black	Dry, cloudless	0,0,0	#000000
Red	Low-mid level clouds with dry atmosphere	255,0,0	#FF0000
Magenta	Mid-level clouds with humid atmosphere at low-mid level	255,0,255	#FF00FF
Green	Moisture of high level	0,255,0	#00FF00
Blue	Moisture of mid-level	0,0,255	#0000FF
Cyan	Moisture of mid-high level	0,255,255	#00FFFF

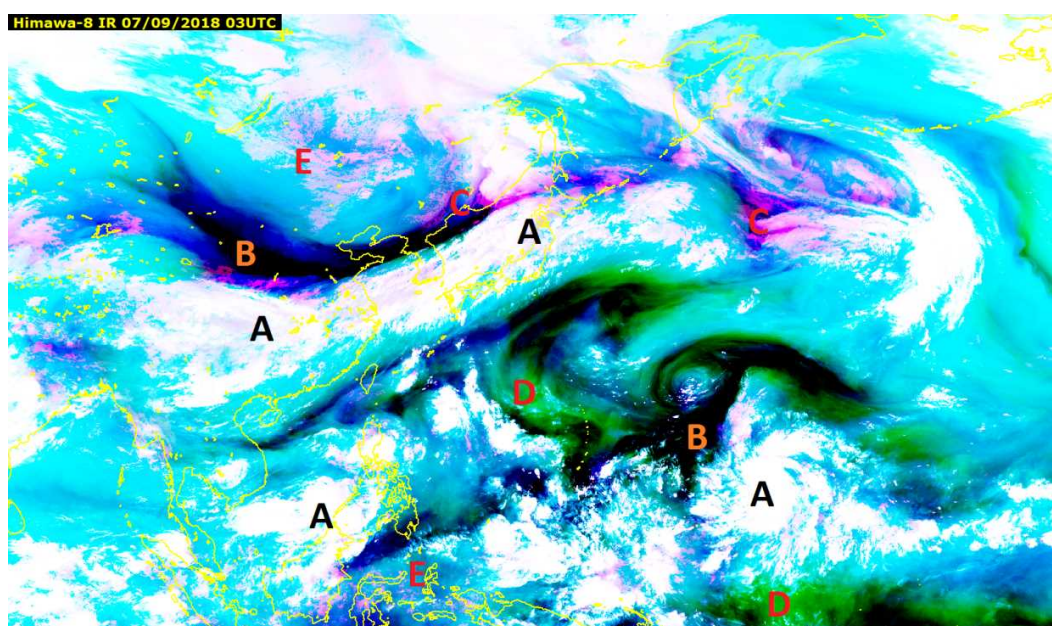


Fig. 25: Example of Simple Water Vapor RGB imagery and related interpretation (0300 UTC, 7 September 2018)

A: clouds with high-level top; B: dry or cloudless area; C: mid-level clouds with humid atmospheric conditions at low/mid-level; D: high-level moisture; E: mid/high-level moisture

13 and the blue beam of Band 10. High-level moisture appears greenish due to medium-high contribution from the green beam of Band 8, while mid-level moisture appears blueish due to

medium/high contribution from the blue beam of Band 10. Mid/high-level moisture appears cyan due to high contributions from the green beam of Band 8 and the blue beam of Band 10. Figure 25

shows an example of Simple Water Vapor RGB imagery and related interpretation, and Fig. 26 shows another (common to Fig. 23). This RGB supports the visualization of water vapor distribution at mid/high levels.

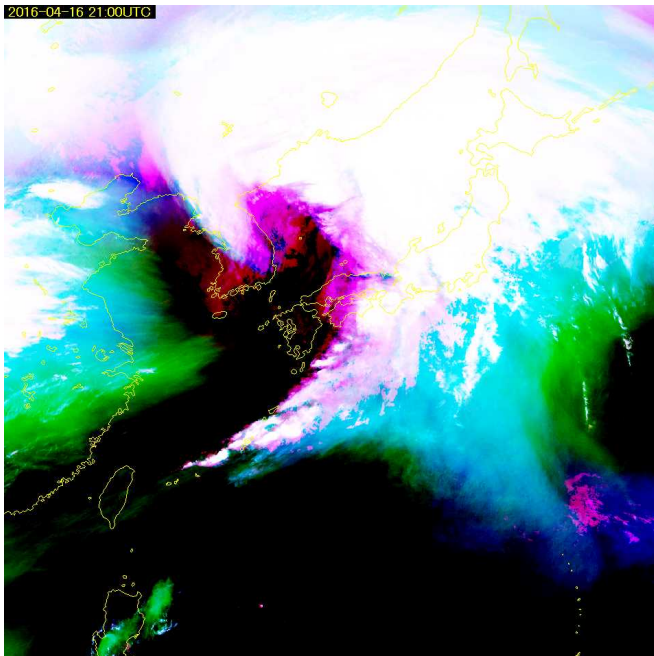


Fig. 26: A developing low around the Korean Peninsula (2100 UTC, 16 April 2016)

4.2. Differential Water Vapor RGB

The Differential Water Vapor RGB developed and proposed by Shimizu (2016) allows analysis of vertical water vapor distribution associated with troughs, ridges and darkening at mid/high levels. It provides more information about dry areas than Simple Water Vapor RGB (Fig. 27).



Fig. 27: A developing low around the Korean Peninsula (2100 UTC, 16 April 2016). The dark-orange streak indicated by the black arrow to the vortex-shaped cloud area with the developing low appears to be a dry intrusion.

Table 25 shows the formation of red/green/blue beams assigned to the RGB. The difference image of the Band 10 (7.3 μm) – Band 8 (6.2 μm) ($\text{BTD}_{\text{B10-B08}}$) range assigned to the red beam indicates vertical (mid to high-level) water vapor distribution. Dry atmospheric conditions exhibit low or almost-zero values (with high contribution for the red beam), while moist conditions exhibit positive values (with relatively lower contribution for the red beam) in $\text{BTD}_{\text{B10-B08}}$ imagery. This also highlights thick

Table 25: Band components and related specifications for Differential Water Vapor RGB

Color	AHI Bands	Central wave length [μm]	Physically relates to	Smaller contribution to the signal of	Larger contribution to the signal of
Red	B10-B08	7.3-6.2	Vertical water vapor distribution Mid-high level clouds	Mid-level humidity Mid-level clouds	Dry upper levels High-level clouds
Green	B10	7.3	Water vapor distribution at Mid-level	Dry Mid-levels Warm brightness temperatures	Moist Mid-levels Cold brightness temperatures
Blue	B08	6.2	Water vapor distribution at upper level	Dry upper levels Warm brightness temperatures	Moist upper levels Cold brightness temperatures

Table 26: Color interpretation and RGB values for Differential Water Vapor RGB

Color	Interpretation	RGB Value	HTML
	Clouds with high level top	255,255,255	#FFFFFF
	Moisture of high level	166,194,232	#A6C2E8
	Dry at high level and moisture at mid-level atmosphere	239,208,68	#EFD044
	Dry at mid-high level atmosphere	255,90,0	#FF5A00

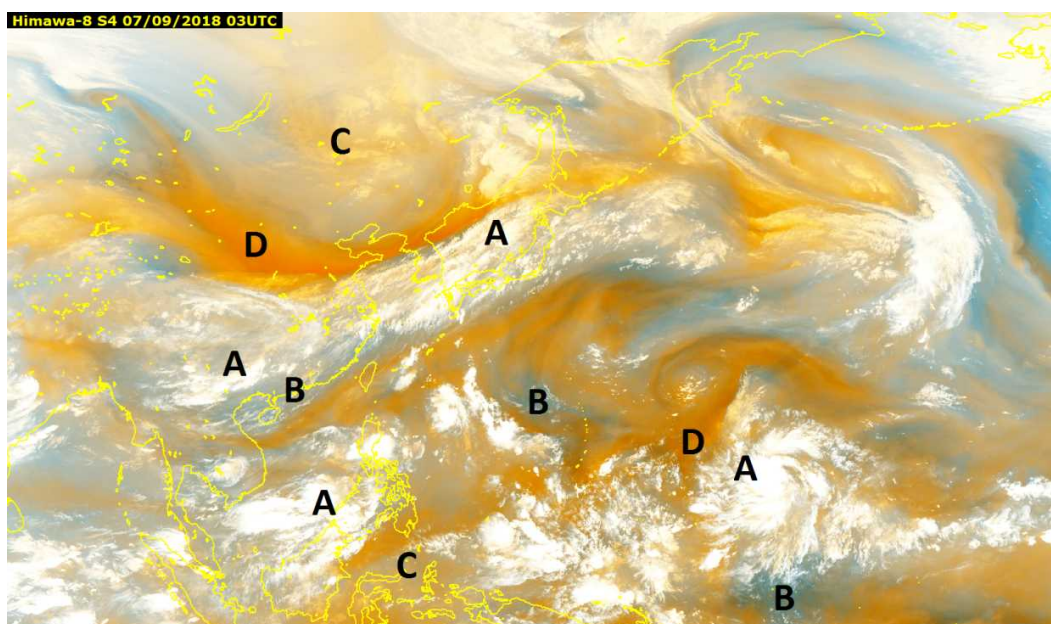


Fig. 28: Example of Differential Water Vapor RGB imagery and related interpretation (0300 UTC, 7 September 2018)

A: clouds with high-level top; B: high-level moisture; C: high-level dryness and mid-level atmosphere moisture; D: mid/high-level atmosphere dryness

high clouds as with the red beams of Day Convective Storm RGB and Airmass RGB. Water vapor imagery from Band 10 (7.3 μm) and Band 8 (6.2 μm) assigned to the green beam and the blue beam of the RGB indicate water vapor distribution in the mid- and upper-level troposphere, respectively, making it suitable both for daytime and nighttime analysis.

Color interpretation for Differential Water Vapor RGB is shown in Table 26. Clouds with a high-level top appear bright whitish due to high contributions from all color beams. High-level moisture appears greyish blue due to medium/high contributions from all color beams.

The shade of blue depends on the blue beam contribution, corresponding to high-level humidity. Dryness in the high-level atmosphere and moisture in the mid-level atmosphere appear yellowish-orange due to high contributions from the red beam of $\text{BTD}_{\text{B10-B08}}$ and the green beam of Band 10. The shade of orange depends on the green beam contribution, corresponding to mid-level humidity. Dryness in the mid/high-level atmosphere appears reddish due to high contribution from the red beam of $\text{BTD}_{\text{B10-B08}}$. Figure 28 shows an example of Differential Water Vapor RGB imagery and related interpretation.

4.3. Cloud Phase Distinction RGB

Table 27: Band components and related specifications for Cloud Phase Distinction RGB

Color	AHI Bands	Central wave length [μm]	Physically relates to	Smaller contribution to the signal of	Larger contribution to the signal of
Red	B13	10.4	Cloud top temperature	Warm clouds	Cold clouds
Green	B03	0.64	Cloud optical thickness	Thin clouds	Thick clouds Snow covered land Sea ice
Blue	B05	1.6	Cloud phase Snow and ice	Ice clouds	Water clouds

Table 28: Color interpretation and RGB values for Cloud Phase Distinction RGB

Color	Interpretation	RGB Value	HTML
Yellow	Thick high level clouds with ice particles, Cb	255,255,0	#FFFF00
Orange	Thin high level clouds with ice particles	255,125,65	#FF7D41
Bright Green	Thick low level ice clouds Snow/ice covered area	0,255,0	#00FF00
Cyan	Thick low level water clouds	0,255,255	#00FFFF

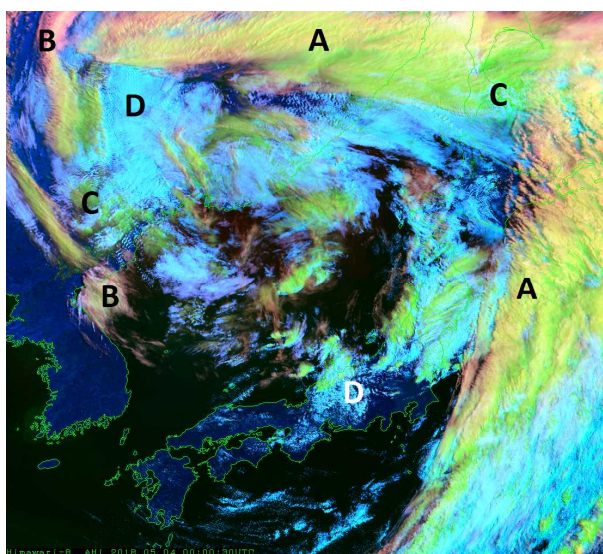


Fig. 29: Cloud area associated with a polar-low pressure system around the Sea of Japan (0000 UTC, 4 May 2018)

A: thick high-level clouds with ice particles;
 B: thin high-level clouds with ice particles (the lower “B” corresponds to high-level lee cloudiness);
 C: thick low-level ice clouds;
 D: thick low-level water clouds

JMA’s Cloud Phase Distinction RGB consists of the red/green/blue assigned to the imagery of Band 13 (10.4 μm), Band 3 (0.64 μm) and Band 5 (1.6 μm), making it suitable for daytime analysis. It allows simultaneous analysis of cloud thickness (Band 3), cloud top height (Band 13) and cloud phase (Band 5) (Table 27).

Color interpretation for Cloud Phase Distinction RGB is shown in Table 28. Thick high-level clouds with ice particles appear yellowish due to high contributions from the red beam of Band 13 and the green beam of Band 3. Thin high-level clouds with ice particles appear orange due to high contribution from the red beam of Band 13 and medium contribution from the green beam of Band 3. Thick low-level ice clouds and snow/ice-covered areas appear bright greenish due to principally high contribution from the green beam of Band 3. Thick low-level water clouds appear cyan due to high contributions from the green beam of Band 3 and the blue beam of Band 5.

Figure 29 shows an example of Cloud Phase Distinction RGB imagery and related

interpretation (as per Fig. 11 for Day Microphysics RGB). Although this product is not particularly superior for detailed analysis of cloud physics, it eliminates the need for complex calculation regarding the reflective part of Band 7. Cb clouds with thick, high content often appear in a saturated yellowish hue due to excessive emphasis (Fig. 30), but clear bluish low-level clouds in this case support determination of low-level movement.

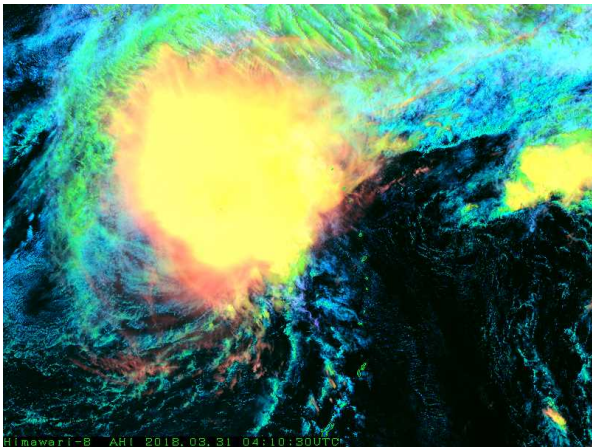


Fig. 30: Typhoon Jelawat (T1803) around the Mariana Islands (0410 UTC, 31 March 2018)

4.4. Day Cloud Phase RGB

EUMETSAT’s Day Cloud Phase RGB is similar to Natural Color RGB except for the green beam (Table 29), allowing superior discrimination of cloud particle phase based on the characteristic near-infrared Band 6 (2.3 μm). It is composed of the red/green/blue assigned to the imagery of

Band 5 (1.6 μm), Band 6 and Band 1 (0.47 μm). The blue beam of Band 1 can be replaced with Band 3 data (0.64 μm). Accordingly, this RGB scheme is suitable for daytime analysis. The near-infrared imagery from Band 5 assigned to the red beam of the RGB supports determination of ice/water cloud particle phase, with reflectivity being lower for the former. The near-infrared imagery from Band 6 assigned to the green beam supports determination of cloud particle phase and size, with reflectivity being lower for large ice particles. As particle size analysis is qualitative and only a rough guide, further detailed examination is required in future research. The visible imagery from Band 1 assigned to the blue beam indicates cloud optical thickness.

Color interpretation for Day Cloud Phase RGB is shown in Table 30. Ice clouds with small particles appear bright blue due to generally high contributions from the green beam of Band 6 and the blue beam of Band 1, while ice clouds with large particles appear dark blue due to principally high contributions from the blue beam of Band 1. Water clouds with small particles appear bright warm yellow due to generally high contributions from the red beam of Band 5 and the green beam of Band 6. Water clouds with large particles appear purple due to generally high contributions from the red beam of Band 5 and the blue beam of Band 1.

Figure 31 compares a cloud area with a low-pressure (polar low) system around the Sea of

Table 29: Band components and related specifications for Day Cloud Phase RGB

Color	AHI Bands	Central wave length [μm]	Physically relates to	Smaller contribution to the signal of	Larger contribution to the signal of
Red	B05	1.6	Cloud phase	Ice clouds	Water clouds
Green	B06	2.3	Cloud phase and size	Ice clouds with large ice crystals	Thick water clouds with small droplets
Blue	B01	0.47	Cloud optical thickness	Thin clouds	Thick clouds Snow covered land Sea ice

Table 29: Band components and related specifications for Day Cloud Phase RGB

Color	Interpretation	RGB Value	HTML
	Ice clouds with small particles	70,142,255	#468EFF
	Ice clouds with large particles	45,85,200	#2D55C8
	Water clouds with small particles	255,237,169	#FFEDA9
	Water clouds with large particles	183,101,203	#B765CB

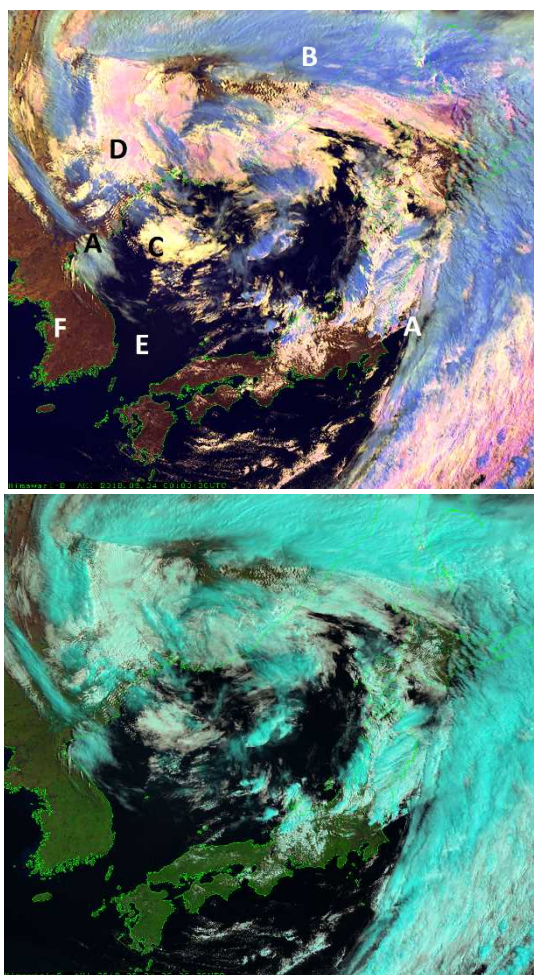


Fig. 31: Comparison involving a cloud area associated with a polar low-pressure system around the Sea of Japan between Day Cloud Phase RGB (top) and Natural Color RGB (bottom) (0000 UTC, 4 May 2018)

A: thick ice clouds with small particles; B: thick ice clouds with large particles; C: thick low-level water clouds with small particles; D: thick low-level water clouds with large particles; E: sea surface; F: land surface

Japan between Day Cloud Phase RGB with related interpretation (upper) and Natural Color RGB (lower) as per Fig. 11 for Day Microphysics RGB and Fig. 29 for Cloud Phase Distinction RGB. Day Cloud Phase RGB facilitates determination of cloud phase and particle size. However, excessive ice cloud appearance is often seen in Natural Color RGB imagery. In particular, cloud phase determination for “D” here appears more appropriate than with Natural Color RGB. Figure 32 shows the situation for a typhoon as per Figs. 13 and 30. The phases for Cb cloud top and low-level cloud are clear in this imagery.

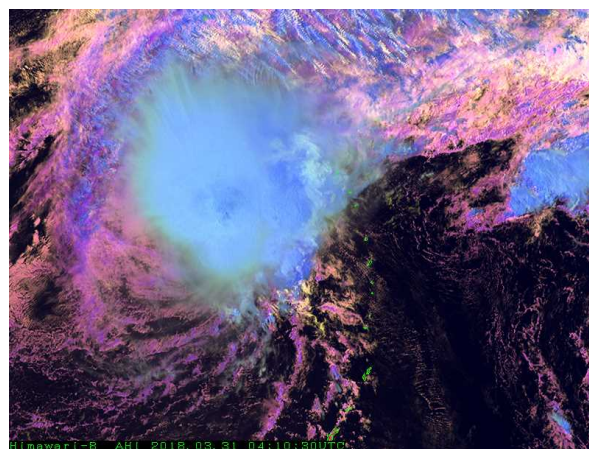


Fig. 32: Typhoon Jelawat (T1803) around the Mariana Islands (0410 UTC, 31 March 2018)

4.5. Day Deep-Cloud RGB

Day Deep-Cloud RGB (Day Convection JMA ver. 1 RGB) developed and proposed by Shimizu (2016) highlights thick clouds such as the Cb variety with overshooting tops based on data from conventional successor bands of the previous MTSAT generation of satellites.

Table 31: Band components and related specifications for Day Deep Clouds RGB

Color	AHI Bands	Central wave length [μm]	Physically relates to	Smaller contribution to the signal of	Larger contribution to the signal of
Red	B13-B08	10.4-6.2	Cloud top temperature	Thin clouds	Thick clouds (with overshooting tops)
Green	B03	0.64	Cloud optical thickness Rough texture of cloud tops	Thin clouds	Thick clouds
Blue	B13 (inverse)	10.4	Cloud top temperature Temperature of surface	Cold clouds	Warm surface

Table 32: Color interpretation and RGB values for Day Deep Cloud RGB

Color	Interpretation	RGB Value	HTML
	Thick clouds	255,0,0	#FF0000
	Thick clouds with overshooting tops	255,255,0	#FFFF00
	Thin high clouds	0,32,96	#002060
	Land/Ocean	0,0,255	#0000FF

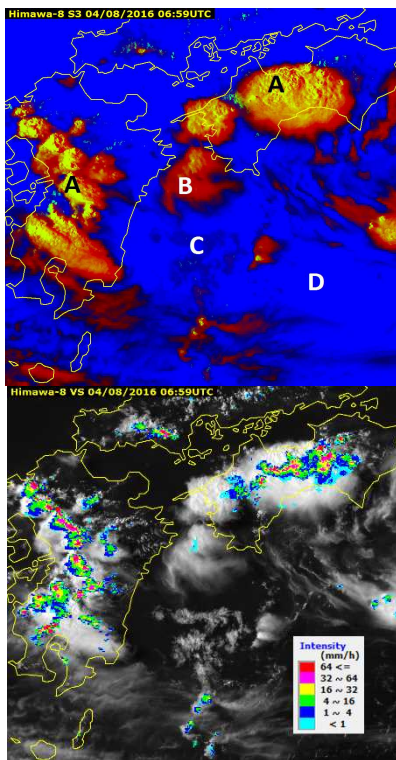


Fig. 33: Comparison case of convective clouds around Japan between Day Deep Cloud RGB imagery (top) and visible image (B03) with radar intensity (bottom) (0700 UTC, 4 August 2016)

A: thick clouds with overshooting tops; B: thick clouds; C: thin high clouds; D: sea surface

Table 31 shows the formation of the red/green/blue beams assigned to the RGB. The difference imagery of the Band 13 (10.4 μm) – Band 8 (6.2 μm) ($BTD_{B13-B08}$) range assigned to the red beam of the RGB helps users to distinguish thick clouds such as Cb and thick multi-layered cloud area. Thick clouds exhibit low or almost-zero values (with high contribution for the red beam) in $BTD_{B13-B08}$ imagery, and thick clouds with overshooting tops tend to exhibit negative values (with higher contribution for the red beam). Visible imagery from Band 3 assigned to the green beam indicates cloud optical thickness and supports visualization for the rough texture of Cb cloud top. As a result, this RGB scheme can be used for daytime analysis. As with 24-hour Microphysics RGB and other products, Band 13 assigned to the blue beam provides inverted IR imagery (with warm pixels contributing blue to RGB imagery).

Color interpretation for Day Deep-Cloud RGB is shown in Table 32. Thick clouds appear red due to high contribution from the red beam of $BTD_{B13-B08}$. Thick clouds with overshooting tops appear yellow or orange due to high contributions from the red beam of $BTD_{B13-B08}$

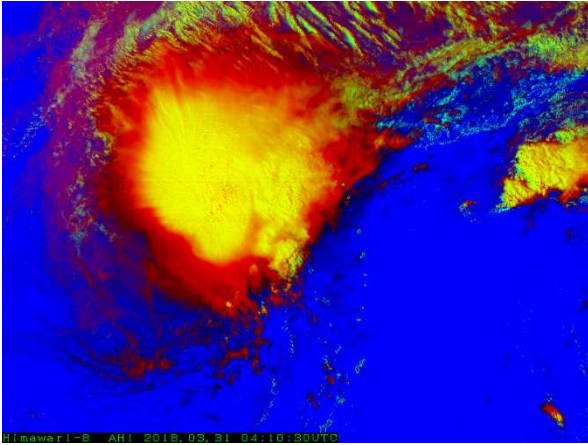


Fig. 34: Typhoon Jelawat (T1803) in the vicinity of the Mariana Islands (0410 UTC, 31 March 2018)

and the green beam of Band 3. Thin high clouds appear dark bluish due to generally low contributions from the red beam of $BTD_{B13-B08}$ and the green beam of Band 3. Land/ocean areas appear blue due to high contribution from the blue beam of Band 13.

Figure 33 compares convective clouds around Japan based on Day Deep-Cloud RGB (top) and visible imagery (B03) with radar intensity (bottom). Thick clouds with overshooting tops appear yellowish with an uneven (red-shadowed) texture (marked “A”). Strong precipitation is observed in these areas. Figure 34 shows Typhoon Jelawat (T1803) as per Figs. 13, 30 and 32. This RGB does not provide the details of cloud particle size and phase supplied by other RGB composites, but does support the

identification of thick convective clouds.

4.6. Natural Fire Color RGB

Natural Fire Color RGB is provided and used by LEO satellite research operators such as NOAA and the Cooperative Institute for Research in the Atmosphere (CIARA). Based on data from the near-infrared Band 6 ($2.3 \mu\text{m}$) of the AHI on board Himawari-8, this scheme is now available in conjunction with Himawari-8’s frequent observation data.

Table 33 shows the formation of the red/green/blue beams assigned to the imagery of Band 6, Band 4 ($0.8 \mu\text{m}$) and Band 3 ($0.64 \mu\text{m}$). This scheme is similar to Natural Color RGB except for the red beam, and while it enables detection of fire hotspots based on the characteristic near-infrared Band 6, it does not readily support discrimination of water/ice clouds. The near-infrared image of Band 6 assigned to the red beam of the RGB supports the detection of fire hotspots such as forest fires and wild fires. These hotspots exhibit high values in Band 6 imagery even during nighttime hours. The near-infrared imagery of Band 4 assigned to the green beam provides sensitivity for vegetation and burn scarring. The visible imagery of Band 3 assigned to the blue beam supports identification of smoke, and indicates cloud optical thickness as with the green beam of Band 4.

Color interpretation for Natural Fire Color RGB is shown in Table 34. Hotspots appear in red due

Table 33: Band components and related specifications for Natural Fire Color RGB

Color	AHI Bands	Central wave length [μm]	Physically relates to	Smaller contribution to the signal of	Larger contribution to the signal of
Red	B06	2.3	Temperature Clouds	Thin clouds	Fire hotspots Thick clouds
Green	B04	0.86	Cloud optical thickness Green vegetation	Thin clouds Burn scar	Thick clouds Vegetation Snow covered land Sea ice
Blue	B03	0.64	Cloud optical thickness	Thin clouds Burn scar	Thick clouds Snow covered land Sea ice Smoke

Table 34: Color interpretation and RGB values for Natural Fire Color RGB

Color	Interpretation	RGB Value	HTML
	Fire hotspots	255,0,0	#FF0000
	(Healthy) vegetation	13,85,39	#0D5527
	Burn scars	90,50,20	#5A3214
	Smoke	15,95,116	#0F5F74
	Clouds	95,245,245	#5FF5F5

to high contribution from the red beam of Band 6, healthy vegetation appears greenish due to high contribution from the green beam of Band 4, and burn scarring appears darker due to low contributions from all beams. Smoke appears bluish due to medium contributions from the green beam of Band 4 and the blue beam of Band 3. Clouds appear cyan due to high contributions from the green beam of Band 4 and the blue beam of Band 3.

In Fig. 36, which shows a forest fire on Sumatra Island in Indonesia, fire hotspots are not clear but smoke plumes are.

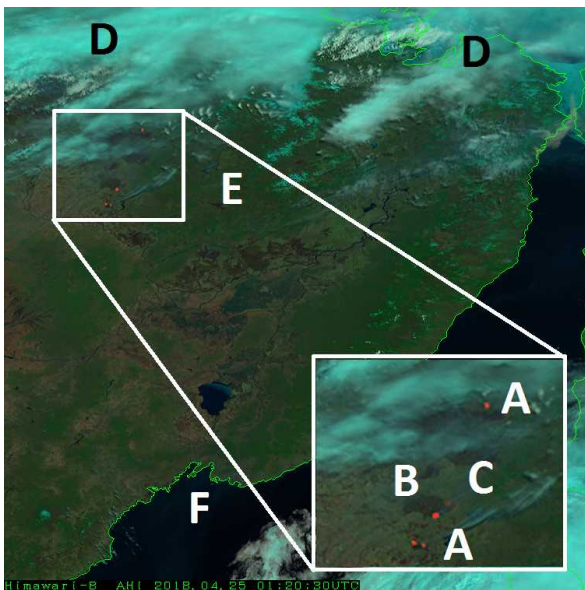


Fig. 35: Forest fire in the vicinity of Siberia, Russia (0120 UTC, 25 April 2018)
 A: fire hotspots; B: burn scars; C: smoke; D: clouds; E: vegetation; F: sea surface

Figure 35 shows an example depicting a forest fire in the vicinity of Siberia. Distinct red pixels indicate fire hotspots, but smoke plumes originating from the fire are not clearly shown.

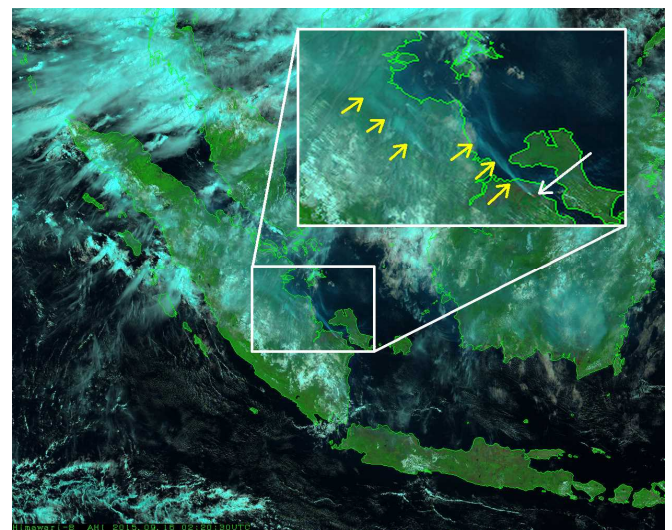


Fig. 36: Forest fire and smoke on Sumatra Island, Indonesia (0220 UTC, 16 September 2015)
 The white arrow indicates a fire hotspot, and the yellow arrows indicate smoke plumes.

4.7. Fire Temperature (Fire Intensity) RGB

Fire Temperature RGB imagery are used and provided by LEO satellite researchers such as CIRA. The near-infrared Band 6 (2.3 μm) of Himawari-8 allows application of this useful scheme to frequent imagery from the GEO satellite as with the Natural Fire Color RGB described in the previous section.

Table 35 shows the formation of red/green/blue beams assigned to the RGB for the imagery of Band 7 (3.9 μm), Band 6 and Band 5 (1.6 μm).

Table 35: Band components and related specifications for Fire Temperature RGB

Color	AHI Bands	Central wave length [μm]	Physically relates to	Smaller contribution to the signal of	Larger contribution to the signal of
Red	B07	3.9	Temperature Cloud phase	Thick water clouds	Fire hotspots (with lower temperature)
Green	B06	2.3	Temperature Cloud phase and size	Thin ice clouds with large ice particles	Fire hotspots (with mid temperature) Thick water clouds with small droplets
Blue	B05	1.6	Temperature Cloud phase	Thin ice clouds	Fire hotspots (with higher temperature) Thick water clouds

Table 36: Color interpretation and RGB values for Fire Temperature RGB

Color	Interpretation	RGB Value	HTML
	Low temperature hotspots	255,0,0	#FF0000
	Medium temperature hotspots	255,255,0	#FFFF00
	High temperature hotspots	255,255,255	#FFFFFF
	Water clouds	85,162,250	#55A2FA
	Ice clouds	0,220,166	#00DCA6

The scheme enables detection of fire hotspots with colors relating to temperature from the data of these thermally sensitive bands.

Hotspot temperatures theoretically depend on Wien's displacement law, which states that the peak wavelength of a blackbody radiator can be calculated using its temperature and a constant.

$$\lambda_{max} = \frac{b}{T} \quad (2)$$

Here, λ_{max} is the peak wavelength [μm], b is Wien's displacement constant (= 2,897) and T is temperature [K]. Thus, warmer black bodies (hotspots in this case) radiate with shorter wavelength peaks. If λ_{max} is 3.9 μm, T is around 743 K (with values of 1,260 K for 2.3 μm and 1,811 K for 1.6 μm). Observed temperatures are actually lower than theoretical black body radiations.

The infrared imagery of Band 7 assigned to the red beam of RGB supports the detection of fire hotspots with relatively low temperatures.

Similarly, the near-infrared imagery of Band 6 assigned to the green beam supports the detection of fire hotspots with relatively medium temperatures, and the near-infrared imagery of Band 5 assigned to the blue beam supports the detection of fire hotspots with relatively high temperatures. Fire hotspots exhibit high values in the respective band imagery even at nighttime in accordance with temperature. In addition, the near-infrared imagery of Band 6 assigned to the green beam supports identification of cloud particle phase (i.e., water or ice) and size, with reflectivity being lower for larger ice cloud particles. The near-infrared imagery of Band 5 assigned to the blue beam of RGB also supports such identification, with reflectivity being lower for ice clouds.

Color interpretation for Fire Temperature RGB is shown in Table 36, with hotspot colors depending on temperature. Low-temperature hotspots appear red due to high contribution from the red beam of Band 7, medium-temperature spots appear yellow due to high contributions

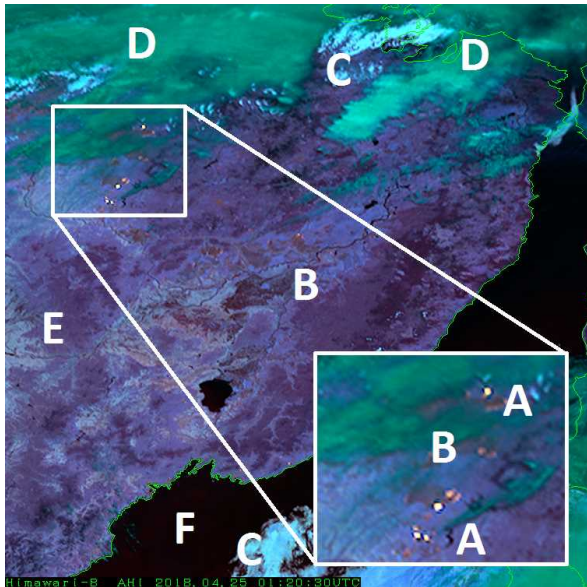


Fig. 37: Forest fire in the vicinity of Siberia, Russia (0120 UTC, 25 April 2018)

A: fire hotspots (relatively high temperature);
 B: fire hotspots (relatively low temperature);
 C: water clouds; D: ice clouds; E: land surface; F: sea surface

from the red beam of Band 7 and the green beam of Band 6, and high-temperature spots appear white due to high contributions from all color beams. Water clouds appear bluish and ice clouds appear greenish due to principally high contributions from the blue beam of Band 5 and the green beam of Band 6, respectively, but smoke is often unclear unlike in True Color RGB and Natural Fire Color RGB.

Figure 37 shows an example of a forest fire in the vicinity of Siberia, Russia (as per Fig. 35). Smoke plumes are less clear than in Natural Fire Color RGB, but fire hotspots with relatively low temperatures are observed (marked “B”). Another example (Fig. 38, as per Fig. 36) also shows distinct yellowish fire hotspot content (white arrow) and reddish fire hotspots (white arrows). In this way, Fire Temperature RGB supports identification of fire hotspots with various colors based on contributions from the three color beams.

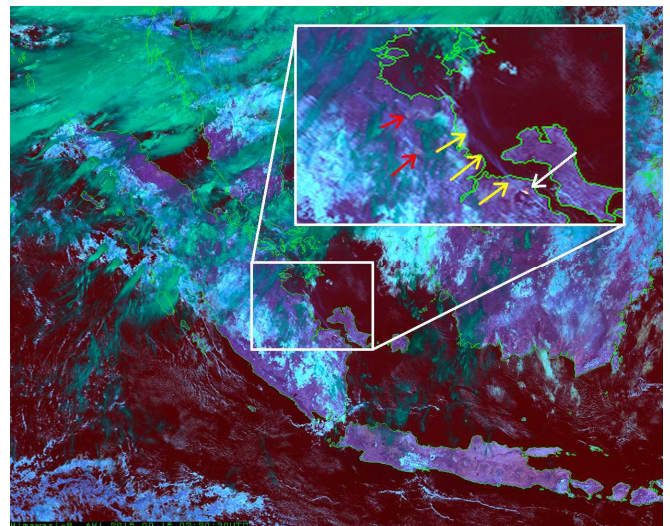


Fig. 38: Forest fire and smoke on Sumatra Island, Indonesia (0220 UTC, 16 September 2015)

The white arrow indicates a fire hot spot (relatively high temperature), red arrows indicate fire hotspots (relatively low temperature) and yellow arrows indicate smoke plumes.

4.8. SO₂ RGB

The toxic sulfur dioxide (SO₂) gas often released naturally by volcanic eruptions can significantly affect human health.

JMA’s SO₂ RGB highlights volcanic SO₂ gas in both daytime and nighttime operation based on data from the SO₂ absorption Band 10 and Band 11.

Table 37 shows the formation of red/green/blue beams assigned to the RGB difference imagery of Band 10 (7.3 μm) – Band 9 (6.9 μm) (BTD_{B10-B09}), Band 11 (8.6 μm) – Band 13 (10.4 μm) (BTD_{B11-B13})/Band 11 (8.6 μm) – Band 14 (11.2 μm) (BTD_{B11-B14}) and Band 13. The scheme is similar to 24-hour Microphysics, with the inclusion of Ash RGB except for the red beam, and allows detection of upper-level SO₂ gas based on the SO₂ absorption characteristic of Band 10. For the green beam, there are two

Table 37: Band components and related specifications for SO2 RGB

Color	AHI Bands	Central wave length [μm]	Physically relates to	Smaller contribution to the signal of	Larger contribution to the signal of
Red	B10-B09	7.3-6.9	SO ₂ gas Thick clouds Vertical water vapor distribution	Thin ice clouds Dry mid-upper levels	Mid-high level SO ₂ gas Thick high level clouds
Green	B11-B13 /B11-B14	8.6-10.4 /8.6-11.2	SO ₂ gas Cloud phase	Thin ice clouds	SO ₂ gas Water clouds
Blue	B13 (inverse)	10.4	Cloud top temperature Temperature of surface	Cold clouds Cold surface	Warm clouds Warm surface

Table 38: Color interpretation and RGB values for SO2 RGB

Color	Interpretation	RGB Value	HTML
	Upper level SO ₂	240,45,0	#F02D00
	Lower level SO ₂	140,240,0	#8CF000
	Lower-upper level SO ₂	220,255,0	#DCFF00
	Thick clouds	150,120,0	#967800
	Thin high level clouds	5,2,20	#050214
	Low level clouds	5,200,90	#05C85A

appropriate combinations in comparison with MSG’s Channel 9 (10.8 μm) – Channel 7 (8.7 μm) as well as the 24-hour Microphysics scheme. Related difference images enable identification of cloud phase, dust and volcanic gas (SO₂). The contrast of BTDB₁₁₋₁₄ difference values for water/ice clouds is superior to that of BTDB₁₁₋₁₃, making it preferable as the green band for SO₂ RGB. The blue beam of Band 13 provides information on surface and cloud top temperatures.

The BTDB₁₀₋₀₉ range assigned to the red beam of the RGB supports the detection of mid/high-level SO₂ gas plumes in the atmosphere. Signal values from BTDB₁₀₋₀₉ are small for SO₂, and the red beam of this RGB indicates thick high clouds with low values. The BTDB₁₁₋₁₃/BTDB₁₁₋₁₄ ranges assigned to the green beam of the RGB are useful in distinguishing between water clouds and ice clouds, as with Ash RGB. SO₂ gas can also be detected based on the related absorption properties in Band 11. As with Ash RGB, Band 13 assigned to the blue beam is used for inverted IR imagery (with warm pixels contributing blue

to RGB imagery).

Color interpretation for SO₂ RGB is shown in Table 38. Upper-level SO₂ gas plumes appear reddish or orange due to principally high contribution from the red beam of BTDB₁₀₋₀₉, lower-level SO₂ appears greenish due to principally high contribution from the green beam of BTDB₁₁₋₁₃/BTDB₁₁₋₁₄, and SO₂ ranging over layers appears yellowish due to high contributions from the red beam of BTDB₁₀₋₀₉ and the green beam of BTDB₁₁₋₁₃/BTDB₁₁₋₁₄. Thick clouds appear yellowish-brown due to medium contributions from the red beam of BTDB₁₀₋₀₉ and the green beam of BTDB₁₁₋₁₃/BTDB₁₁₋₁₄. Thin high-level clouds appear dark due to low contributions from all color beams. Low-level clouds appear greenish (as with lower-level SO₂) due to principally high contribution from the green beam of BTDB₁₁₋₁₃/BTDB₁₁₋₁₄.

Figure 39 shows an eruption of Mt. Merapi in Indonesia as per the examples for True Color RGB (Fig. 9) and Ash RGB (Fig. 20). The greenish area indicated by the white arrow

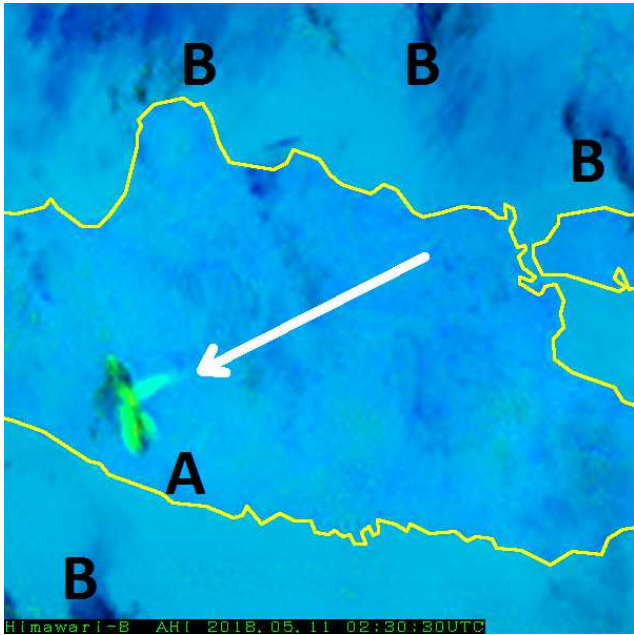


Fig. 39: Eruption of Mt. Merapi, Indonesia (0230 UTC, 11 May 2018). The white arrow indicates the volcanic plume.
A: volcanic SO₂; B: thin cirrus cloud

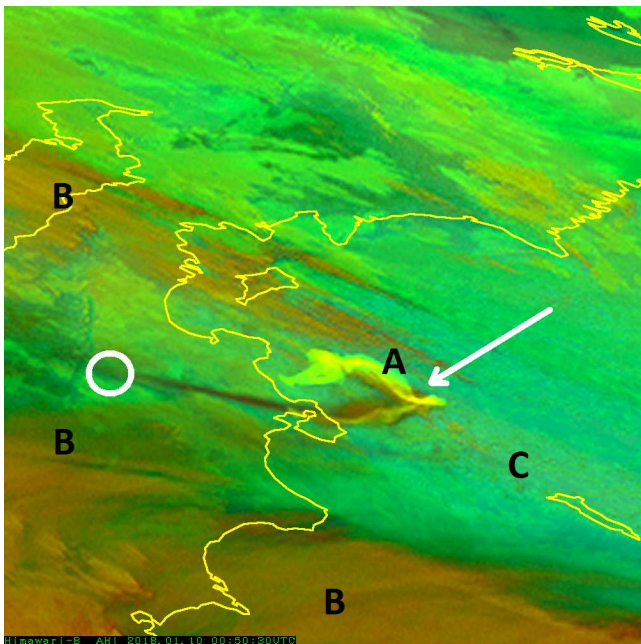


Fig. 40: Eruption of Mt. Shiveluch, Russia (0050 UTC, 10 January 2018). The white circle and white arrow indicate Mt. Shiveluch and the related volcanic plume, respectively.
A: volcanic SO₂; B: thick cloud, C: low-level cloud

corresponds to a volcanic SO₂ gas plume, which appears to be drifting at a relatively lower atmospheric level according to color interpretation. Figure 40 shows an eruption of Mt. Shiveluch in Russia as per the example for Ash RGB (Fig. 21). The yellowish gas plume indicated by the white arrow appears to be exhibiting mid-level drift across the Kamchatka Peninsula. Figure 41 shows an eruption of Mt. Manam in Papua New Guinea as per the examples for Airmass RGB and Ash RGB (Fig. 24). The reddish area marked by the white arrow appears to be a high-level volcanic gas plume.

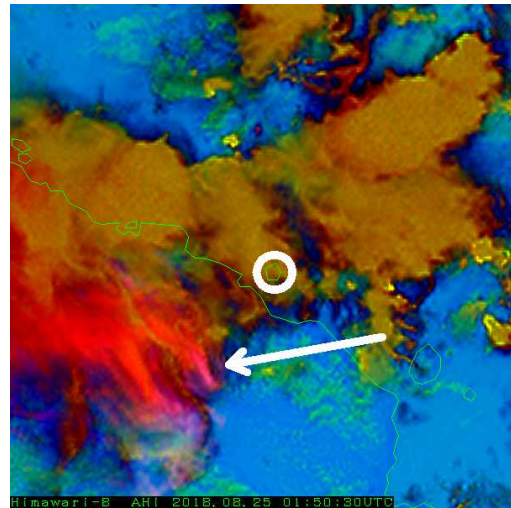


Fig. 41: Eruption of Mt. Manam, Papua New Guinea (0150 UTC, 25 August 2018)
The white circle and white arrow indicate Mt. Manam and the related volcanic plume with SO₂ (reddish area), respectively.

4. Summary

This report outlines a red/green/blue (RGB) composite technique allowing effective analysis based on color shading to reflect various characteristics in Himawari-8 imagery, with coverage including widely used RGBs, LEO RGBs and new RGBs. Standard RGBs based on MSG RGB recipes (such as Night Microphysics

RGB and Dust RGB) are helpful to Himawari-8 imagery users, and other RGBs (such as Natural Fire Color RGB and SO₂ RGB) are also applicable to specific purposes. As related thresholds and color interpretations are still being examined, further research is necessary.

As RGB composite imagery is a qualitative product, its use in combination with quantitative products (e.g., satellite-derived content) is recommended (WMO, 2012).

Acknowledgement

The reviewers' suggestions for optimal content in this report are very much appreciated.

References

- Clerbaux C., Drummond J.R., Flaud J. and Orphal J., 2011: Remote Sensing of Tropospheric Composition from Space, Chapter 3 Thermal Infrared: Absorption and Emission –Trace Gases and Parameters, 137, available at http://www.iup.uni-bremen.de/materials/remensingbook/03_Remote_Sensing_Thermal_IR.pdf
- EUMeTrain, 2017-2018: EUMeTrain Quick Guides, available at http://www.eumetrain.org/rgb_quick_guides/index.html(Accessed 20 October 2018)
- Kerkmann J., 2005: Applications of Meteosat Second Generation (MSG) RGB Images: Part 03 Channel Selection and Enhancements, 2-27, available at http://oiswww.eumetsat.org/WEBOPS/msg_interpretation/PowerPoints/Channels/rgbpart03_20050203.ppt (Accessed 20 October 2018)
- Kerkmann J., 2005: Applications of Meteosat Second Generation (MSG) RGB Images: Part 04 RGB Composites with Channels 01-11 and Their Interpretation, 2-81, available at http://oiswww.eumetsat.org/WEBOPS/msg_interpretation/PowerPoints/Channels/rgbpart04_20050420.ppt (Accessed 20 October 2018)
- Lensky, I.M. and Rosenfeld, D, 2008: Clouds-Aerosols-Precipitation Satellite Analysis Tool (CAPSAT), Atmos.Chem.Phys., 8,6739–6753, available at <https://www.atmos-chem-phys.net/8/6739/2008/acp-8-6739-2008.html> (Accessed 20 October 2018)
- Murata, H., Shimizu, A., 2017: Adjusting SEVIRI RGB Recipes for AHI, WMO RGB Experts and Developers Workshop 2017 (7-9 November 2017, Tokyo, Japan), available at http://www.wmo.int/pages/prog/sat/meetings/documents/RGB-WS-2017_Doc_01a_Adjusting-SEVIRI-RGB-recipes-for-AHI-share.pdf (Accessed 20 October 2018)
- NASA SPoRT, 2017-2018: NASA SPoRT Training Quick Guides, available at <https://nasasporttraining.wordpress.com/quick-guides/> (Accessed 20 October 2018)
- Shimizu, A., 2017: Newly proposed RGBs by Himawari-8 and some case studies, WMO RGB Experts and Developers Workshop 2017 (7-9 NOVEMBER 2017, Tokyo, Japan), available at http://www.wmo.int/pages/prog/sat/meetings/documents/RGB-WS-2017_Doc_02a_Newly-proposed-RGBs-by-Himawari-8-20171106.pdf (Accessed 20 October 2018)

Shimizu, A., Saitou, K., Yamamoto, M., 2017:
Image characteristics of the 16 bands of
Himawari-8's AHI, Meteorological Satellite
Center technical note, 39-69. (in Japanese)

WMO, 2007: RGB composite satellite imagery
workshop final report (5-6 June 2007 Boulder,
CO, U.S.A.), available at
[http://www.wmo.int/pages/prog/sat/documents
/RGB-1_Final-Report.pdf](http://www.wmo.int/pages/prog/sat/documents/RGB-1_Final-Report.pdf) (Accessed 20
October 2018)

WMO, 2012: WMO/EUMETSAT workshop on
RGB satellite products final report (17-19
September 2012, Seeheim, Germany),
available at
[http://www.wmo.int/pages/prog/sat/documents
/RGB-WS-2012_FinalReport.pdf](http://www.wmo.int/pages/prog/sat/documents/RGB-WS-2012_FinalReport.pdf) (Accessed
20 October 2018)

Appendix 1. Widely used RGB composites and recommended thresholds for EUMETSAT MSG data

Note: The infrared channels of MSG/SEVIRI (CH4 – CH9) are shown in inverse imagery (i.e., bright pixels correspond to high-TBB pixels).

	MSG channels	Central wave length [μm]	Min [K/%]	Max [K/%]	Gamma
Natural Color RGB					
R	CH03	1.6	0%	100%	1.0
G	CH02	0.8	0%	100%	1.0
B	CH01	0.6	0%	100%	1.0
Day Snow-Fog RGB					
R	CH02	0.8	0%	100%	1.7
G	CH03	1.6	0%	70%	1.7
B	CH04refl	3.9	0%	30%	1.7
Day Microphysics RGB (Summer/Winter)					
R	CH02	0.8	0%	100%	1.0
G	CH04refl	3.9(summer) /3.9(winter)	0% /0%	60% /25%	2.5 /1.5
B	CH09	10.8	203.0K	323.0K	1.0
Day Convective Storms RGB					
R	CH05-CH06	6.2-7.3	-35.0K	5.0K	1.0
G	CH04-CH09	3.9-10.8	-5.0K	60.0K	0.5
B	CH03-CH01	1.6-0.6	-75%	25%	1.0
Night Microphysics RGB					
R	CH10-CH09	12.0-10.8	-4.0K	2.0K	1.0
G	CH09-CH04	10.8-3.9	0.0K	10.0K	1.0
B	CH09	10.8	243.0K	293.0K	1.0
24-hour Microphysics RGB					
R	CH10-CH09	12.0-10.8	-4.0K	2.0K	1.0
G	CH09-CH07	10.8-8.7	0.0K	6.0K	1.2
B	CH09	10.8	248.0K	303.0K	1.0
Dust RGB					
R	CH10-CH09	12.0-10.8	-4.0K	2.0K	1.0
G	CH09-CH07	10.8-8.7	0.0K	15.0K	2.5
B	CH09	10.8	261.0K	289.0K	1.0
Ash RGB					
R	CH10-CH09	12.0-10.8	-4.0K	2.0K	1.0
G	CH09-CH07	10.8-8.7	-4.0K	5.0K	1.0
B	CH09	10.8	243.0K	303.0K	1.0
Airmass RGB					
R	CH05-CH06	6.2-7.3	-25.0K	0.0K	1.0
G	CH08-CH09	9.7-10.8	-40.0K	5.0K	1.0
B	CH05	6.2	243.0K	208.0K	1.0

Appendix 2. Calculation for Band 7 (3.9 μ m) solar reflectance

The solar component (reflectance) for 3.9 μ m is calculated as

$$R_{refl} = 100 * \frac{(R_{tot} - R_{therm})}{(TOARAD - R_{therm})} \quad (A.1)$$

Here, R_{refl} is reflectance for 3.9 μ m (%), R_{tot} is the measured total radiance [$mWm^{-2}ster^{-1}(cm^{-1})^{-1}$] for 3.9 μ m, R_{therm} is the thermal component of radiance [$mW m^{-2}ster^{-1}(cm^{-1})^{-1}$] for channel 3.9 μ m, and TOARAD is the solar constant at the top of the atmosphere for 3.9 μ m as described below.

Total radiance (R_{tot}) and the thermal component of radiance (R_{therm}) are calculated as follows with a sensor Planck function:

$$R_{tot} = \frac{c_1 v^3}{\{exp[c_2 v / (A + BT_{b3.9} + CT_{b3.9}^2)] - 1\}} \quad (A.2)$$

$$R_{therm} = \frac{c_1 v^3 R_{3.9corr}}{\{exp[c_2 v / (A + BT_{b10.4} + CT_{b10.4}^2)] - 1\}} \quad (A.3)$$

Here, $T_{b3.9}$ is the TBB for 3.9 μ m, $T_{b10.4}$ is the TBB for 10.4 μ m (Band 13), $c_1 = 1.19104 \times 10^{-5}$ [$mWm^{-2}ster^{-1}(cm^{-1})^{-4}$], $c_2 = 1.43878$ [$(cm^{-1})^{-1}$], v is the central wave number ($v = 2575.767$), and A, B and C are constants of the sensor Planck function given by $A = 0.4793907798197780$, $B = 0.999234381214647$ and $C = 1.85684785537253 \times 10^{-7}$. These constants are specific to Himawari-8.

As noted above (A.3), the thermal component of radiance (R_{therm}) can be derived by substituting the TBB for 10.4 μ m with that for 3.9 μ m in the sensor Planck function. This assumption is based on a black-body radiation of $T_{b3.9} = T_{b10.4}$ with no solar radiation.

$R_{3.9corr}$ is a correction term for absorption by CO_2 as given by

$$R_{3.9corr} = \frac{[T_{b10.4} - 0.25(T_{b10.4} - T_{b3.9})]^4}{T_{b10.4}^4} \quad (A.4)$$

However, as absorption by CO₂ can be ignored for Band 7 of AHI/Himawari-8, $R_{3.9corr}$ is 1 for this band.

Thus, A.3 is replaced as follows:

$$R_{therm} = \frac{c_1 v^3}{\{exp[c_2 v / (A + B T_{b10.4} + C T_{b10.4}^2)] - 1\}} \quad (A.3)'$$

The solar constant at the top of the atmosphere for 3.9 μm (TOARAD) is calculated as

$$TOARAD = (C_{3.9}/ESD^2) \cos \theta * \exp \left\{ - \left(1 - R_{3.9corr} \right) \frac{\cos \theta}{\cos \theta_{SAT}} \right\} \quad (A.5)$$

Here, $C_{3.9}$ is a constant depending on the weighting function of 3.9 μm given by $C_{3.9} = 4.8077$, θ is the solar zenith angle, θ_{SAT} is the satellite zenith angle, and ESD is the earth-sun distance (in Astronomical Units) given as

$$ESD(JulianDAY) = 1.0 - 0.0167 \cos(2\pi(JulianDay - 3)/365) \quad (A.6)$$

Here, JulianDAY is the number of days since the beginning of January 1st 4713 B.C. (e.g., January 1st 2019 is 2,458,485).

θ (the solar zenith angle) can be derived from date, time, latitude and longitude values. For twilight conditions (i.e., $\theta > 80^\circ$), it should be set as a conservative value of 80° .

As $R_{3.9corr} = 1$ for Band 7, Equation A.5 can be represented as

$$TOARAD = (C_{3.9}/ESD^2) \cos \theta \quad (A.5)'$$

ひまわり 8 号による RGB 合成画像の紹介

志水 菊広*

要旨

ひまわり 8 号に搭載されている多バンド観測イメージャ AHI (Advanced Himawari Imager) による衛星画像から多くの物理的情報を得ることができるようになった。これらの衛星画像を赤 (Red)、緑 (Green)、青 (Blue) に着色し重ね合わせる RGB 合成技術は、複数の画像の情報を活用する適切な手法の一つである。WMO によって推奨される世界標準の RGB スキームを中心に RGB 合成画像は予報官や研究者の間で広く利用されてきた。今後の参考資料として、本報告は広く使われている RGB 合成画像や当庁で開発された RGB を含めて、ひまわり 8 号画像に適用される RGB 合成技術の基礎的知識について紹介する。

*気象衛星センター データ処理部解析課

(2018 年 11 月 31 日受領、2020 年 10 月 30 日受理)